Band offset formation at semiconductor heterojunctions through density-based minimization of interface energy

Raymond T. Tung[1,*] and Leeor Kronik[2,†]

[1]*Department of Physics, Brooklyn College, CUNY, Brooklyn, New York 11210, USA and Physics Ph.D. Program, Graduate Center, CUNY, New York, New York 10016, USA*

[2]*Department of Materials and Interfaces, Weizmann Institute of Science, Rehovoth 76100, Israel*

(Received 13 May 2016; published 24 August 2016)

It is well known that the magnitude of band offset (BO) at any semiconductor heterojunction is directly derivable from the distribution of charge at that interface and that the latter is decided by a minimization of total energy. However, the fact that BO formation is governed by energy minimization has not been explicitly used in theoretical BO models, likely because the equilibrium charge densities at heterojunction interfaces appear difficult to predict, except via explicit calculation. In this paper, electron densities at a large number of (100), (110), and (111) oriented heterojunctions between lattice-matched, isovalent semiconductors with the zinc blende (ZB) structure have been calculated by first-principles methods and analyzed in detail for possible common characteristics among energy-minimized densities. Remarkably, the heterojunction electron density was found to largely depend only on the immediate, local atomic arrangement. In fact, it is so much so that a juxtaposition of local electron-densities generated in oligo-cells (LEGOs) accurately reproduced the charge densities that minimize the energy for the heterojunctions. Furthermore, the charge distribution for each bulk semiconductor was found to display a striking separability of its electrostatic effect into two neutral parts, associated with the cation and the anion, which are approximately transferrable among semiconductors. These discoveries form the basis of a neutral polyhedra theory (NPT) that approximately predicts the equilibrium charge density and BO of relaxed heterojunctions from the energy minimization requirement. Well-known experimentally observed characteristics of heterojunctions, such as the insensitivity of BO to heterojunction orientation and the identity of interface bonds, the transitivity rule, etc., are all in good agreement with the NPT. Therefore, energy minimization, which essentially decides the electronic properties of all other solid and molecular systems, also governs the formation of the charge density at these heterojunction interfaces. In particular, the approach presented here eliminates the need to invoke mechanisms that are specific to semiconductor interfaces.

DOI: 10.1103/PhysRevB.94.075310

I. INTRODUCTION

The formation of band offsets (BOs) at heterojunctions of semiconductors or insulators is an important issue for condensed matter physics in general and for the design and operation of electronic, optoelectronic, and multiferroic devices based on solid semiconductors and insulators [1,2]. After decades of intensive investigations, however, the basic mechanism responsible for BO formation remains ambiguous [1], as a host of models of different origins appears to predict/explain the experimental BOs similarly [2].

The main quantities pertaining to BO formation are illustrated in Fig. 1, which shows that the valence BO (VBO) at a heterojunction between semiconductors (or insulators) A and B, $\Phi_{\mathrm{VBO}}^{A-B}$, can be decomposed into two bulk terms and one interface term:

$$\Phi_{\mathrm{VBO}}^{\mathrm{A-B}} = E_{\mathrm{VBM}}^{\mathrm{int}}(A) - E_{\mathrm{VBM}}^{\mathrm{int}}(B) = \mu_A - \mu_B + e\Delta_{\mathrm{ISR}}. \tag{1}$$

In the above equation and in Fig. 1, $E_{\mathrm{VBM}}^{\mathrm{int}}$ is the valence band maximum (VBM) position of a semiconductor near the heterojunction interface; $-e\overline{V_{\mathrm{Coul.}}}$ is the averaged electrostatic potential energy (elaborated in detail below); and μ, the internal chemical potential, is the difference between the VBM and $-e\overline{V_{\mathrm{Coul.}}}$ for a semiconductor. Being a purely intensive property, μ is obtainable from a bulk semiconductor calculation with periodic boundary conditions. The interface dipolar term, $e\Delta_{\mathrm{ISR}} = -e\overline{V_{\mathrm{Coul.}}^{A}} + e\overline{V_{\mathrm{Coul.}}^{B}}$, is the difference between the averaged electrostatic potential energies across the interface, where ISR stands for interface-specific region. It is a quantity that may vary with interface specifics, such as atomic structure, orientation, and composition. Being the only term on the right hand side of Eq. (1) that is not known *a priori* for any heterojunction, $e\Delta_{\mathrm{ISR}}$ is both responsible for the magnitude of the VBO and in need of explanation by BO theories.

Experiments have shown that, for the majority of isovalent heterojunctions, the BO is largely independent of atomic structure, orientation, and other specifics of the interface, to the point that the formation of BO has often been called a bulk effect [1,3]. A well-known consequence of such seemingly bulklike behavior is the transitivity rule for BOs that has been observed for some [4–7], though not all [8–11], semiconductors. In the long history of heterojunction research, there have been many models and theories proposed to account for the formation of VBO. Perhaps inspired by bulklike experimental findings, most of these theories involve mechanism(s) beyond the realm of chemistry in order to possess a built-in insensitivity of the BO to interface specifics. Theories can be roughly be categorized into two groups [12]:

*rtung@brooklyn.cuny.edu

†leeor.kronik@weizmann.ac.il

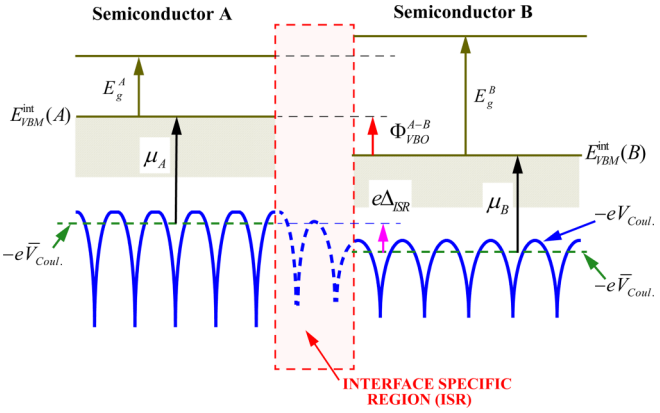

FIG. 1. Potential energy and energy band diagram at a semiconductor heterojunction interface. The lateral ($-eV_{\mathrm{Coul.}}$) and macroscopic ($-e\overline{V_{\mathrm{Coul.}}}$) averages of the electrostatic potential energy (see text for definition) are shown as solid and dashed thick lines, respectively. The internal ionization potential, μ, is the energy difference between the VBM and the macroscopically averaged electrostatic potential energy. $e\Delta_{\mathrm{ISR}}$ is the difference between the bulk values of $-e\overline{V_{\mathrm{Coul.}}}$. $E_g^{A/B}$ is the bandgap of semiconductor A or B, and $\Phi_{\mathrm{VBO}}^{A-B}$ is the valence band offset between the two semiconductors.

those based on certain assumptions on the charge density [13–20] and those based on an assumed fixed internal reference energy level (in the band gap) of the individual semiconductor [21–27]. The former group proposed that a certain charge distribution may be used to represent the bulk semiconductors. When two bulk densities are stacked together, the charge density of the heterojunction is assumed to be approximately reproduced. Perhaps the best example here is the model solid theory [18,19], which uses superimposed densities of neutral atoms to approximately represent the electronic density for each bulk semiconductor, as well as for the interface of the heterojunction. The operation of this type of model then relies on the absence of significant charge rearrangement at the heterojunction during equilibration with respect to the combined charge densities for atoms in isolation. The latter group, exemplified by the proposal of the charge neutrality level (CNL), obtained by generalizing the concept of metal-induced gap states [21], assumes that a discrepancy in the CNLs for two bulk semiconductors drives the distribution of charge and the formation of a dipole at the interface between these two semiconductors, in the direction for the two CNLs to align [28]. However, the thermodynamic basis for charge distribution driven by CNL alignment mechanisms has not been quantitatively spelled out for insulating heterojunctions. An extensive comparison of theoretical predictions with available experimental data identified no clear favorites among all existing theories [2]. Therefore, the basic mechanism responsible for BO formation remains ambiguous [1].

The interface term $e\Delta_{\mathrm{ISR}}$, in Fig. 1 and Eq. (1), which is crucial to the magnitude of the VBO of a heterojunction, is purely electrostatic in nature. It results entirely from the charge distribution in the interface region and has no explicit dependence on the bulk energy band structures of the two semiconductors. For any electronic system, the laws governing the equilibrium charge density distribution are all well known. As perhaps most explicitly stated in the celebrated Hohenberg-Kohn theorem of density functional theory (DFT) [29], the ground-state charge density is known to be that which uniquely defines, and minimizes the energy of, the system's Hamiltonian. It seems reasonable to expect, then, that comprehensive BO theories could be based on, and their main task should be, the accurate prediction/modeling of the spatial distribution of the equilibrium charge density at heterojunction interfaces. The advantage of such a direct, electron-density-based approach toward the explanation of BO, however, has not been seized by many previous computational investigations. Even though predicting the equilibrium charge distribution of a heterojunction seems difficult in general, the present paper shows that this is possible for heterojunctions between semiconductors with the zinc blende (ZB) structure and that the formation of BO in these heterojunctions can be understood based on the requirement that the actual density distribution across the heterojunction has to be the one that minimizes the interface energy.

Interfaces and multilayered structures of semiconductors with ZB and diamond structures have long been in wide use for the fabrication of various devices and the investigation of fundamental phenomena in condensed matter physics. In fact, results obtained from interfaces of these semiconductors have shaped most of the existing ideas on BO formation. The band structure and charge distribution associated with directional, tetrahedral, sp^3 bonds in solids have been the subject of many thorough investigations. Technologically important and well-studied semiconductor heterojunctions are insulating at low temperatures, with the occupied states energetically separated from excited states, e.g., conduction band. The charge distribution relevant for BO formation thus arises only from occupied (i.e., valence) bands. A chemically intuitive view on the formation of the VB for ZB crystals has been provided by the tight binding (TB) approximation, also known as the linear combination of atomic orbitals (LCAO) theory. It begins with the formation of hybrid orbitals for each atom and neighboring cation-anion pair [30], during which the energy of the bond is minimized and the spatial distribution of charge is arrived at. The antibonding orbitals, forming the unoccupied conduction band, may be discarded without affecting either the total energy or the charge distribution for the subsequent transformation of bond orbitals into the VB structure [31,32]. Band features at high symmetry points of ZB semiconductors can be reproduced through these procedures by fitting a small number of parameters, ignoring all interactions beyond second nearest-neighbors and even some second nearest-neighbor interactions. The focus on bonds in TB theory has also been justified through first-principles calculations. Specifically, maximally localized Wannier functions for ZB crystals have been shown to be concentrated between pairs of nearest neighbors at locations of the sp^3 bond orbitals [33,34]. These results suggest that charge distribution of the individual bond may serve as the basic unit in the analysis and modeling of equilibrium charge density not only for bulk semiconductors but also other structures built on a tetrahedral network, such as heterojunction interfaces.

The above focus on bonds is in agreement with the concepts of DFT, which is explicitly centered on the electron density. The basic premise of this paper states that because the local

atomic structure of any part of a tetrahedral heterojunction is essentially identical to that encountered in some bulk or ternary semiconductor, it is plausible that the equilibrium charge densities for the two are similar. Indeed, the present paper shows explicitly that the equilibrium charge density at heterojunctions of semiconductors with ZB structures systematically displays a close relationship with the local atomic structure, which makes the modeling of the interface charge distribution possible and reasonably straightforward: Because the local atomic structure of any part of a heterojunction can be recreated in a bulk unit cell containing a few (i.e., oligo-) units of different ZB materials, the charge density that minimizes the energy of such an oligo-cell then serves as a convenient arena in which the formation of charge density that minimizes the energy of the entire interface can be assessed. Strikingly, the equilibrium charge density of an entire heterojunction is found to be closely approximated by juxtaposition, layer-by-layer or bond-by-bond, of local electron-densities generated in oligo-cells (LEGOs). Detailed analysis of bulk semiconductors then reveals a striking consistency in the equilibrium charge distribution immediately surrounding any particular ion. Specifically, the distribution of charge inside an overall-neutral polyhedron, characterized by the covalent radius along bond directions, is nearly independent of the identity of its bonding partners. This forms the basis of a neutral polyhedra theory (NPT), which we propose here as a means for modeling the charge density at heterojunction interface from the perspective of minimization of interface energy. We find that the BOs of a large number of heterojunctions obtained from first-principles calculations are well reproduced by NPT. The BO formation at these heterojunctions can therefore be understood in terms of the same chemistry that is responsible for charge distribution and bond formation in other electronic systems, without the need to invoke special mechanisms applicable only to solid interfaces.

The article is organized as follows: computational details and the general approach to density analysis are discussed next, followed by results on heterojunctions between semiconductors with a common anion. Unrelaxed heterojunctions between semiconductors without a common element are then discussed. A careful look at the electrostatics of bulk semiconductors with, or constrained to have, the same lattice parameter then takes place, followed by discussion of the BO of relaxed heterojunctions. The rationale for the NPT is then presented and shown to provide reasonable VBO predictions even for relaxed heterojunctions.

II. COMPUTATION AND ANALYSIS

In the present paper, first-principles electronic structure calculations have been conducted on various structures with a ZB lattice, using a plane wave basis and the projector augmented wave (PAW) method, as implemented in the Vienna *Ab initio* Simulation Package (VASP) [35–37]. All systems were calculated within DFT, using the Perdew-Burke-Ernzerhof (PBE) [38] generalized-gradient approximation (GGA) for the exchange-correlation functional. These calculations yield (within the chosen approximate exchange-correlation functional) the ground-state electron density that minimizes the total-energy functional per any given input

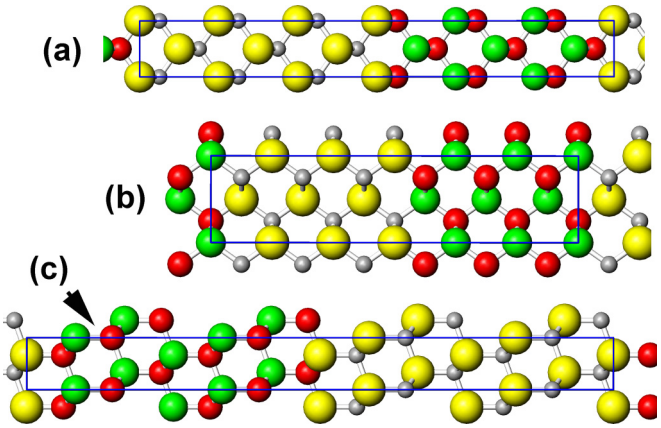

FIG. 2. Ball-and-stick models of structures used in the calculations. Larger and smaller spheres represent anions and cations, respectively. (a) (100) supercell, (b) (110) supercell, and (c) (111) supercell. The outlines of the repeating unit used for the calculation, which contains 12 anions and 12 cations for each interface orientation, are marked.

atomic structure. Selected systems were also computed within the local density approximation (LDA) approach and with different pseudopotentials for comparison. Throughout these comparisons, the main results reported here were found to be essentially independent of functional or pseudopotentials used. The VBOs were calculated from supercells. Ball-and-stick models that were used for (100), (110), and (111) heterojunctions are shown in Fig. 2. As indicated by boxes in the diagrams, each supercell contains 12 cations, six from each of the semiconductors, and 12 anions, which together form two back-to-back interfaces with identical atomic structures for (100) and (110) heterojunctions, and atomic structures that are electrically equivalent for the (111) heterojunction. The sizes of the supercells are adequate, as small increases or decreases in the size of the supercell were found to have a negligible effect on the charge distribution or VBO of the heterojunction. For heterojunctions between two semiconductors with a common element, e.g., GaAs/AlAs heterojunctions, Fig. 2 remains valid as long as the two different types of anions drawn in each diagram are understood to be the same. In addition to supercell calculations, the charge distribution and band structure of bulk semiconductors and the charge distribution of ternary or quaternary compounds with a small number of ZB cells (oligo-cells) were also studied numerically. These are discussed in detail below.

In order to compare the charge distribution at a heterojunction to other reference densities, such as bulk densities, it is advantageous to have a consistent method to zoom in on different parts of the interface for a detailed analysis. To partition the electron density of a multiatomic system into parts associated with each individual atom or bond, several methods in quantum chemistry are available [39–42] based on spatial analysis of the charge density. For ZB systems, however, the bonding electrons are known *a priori* to reside largely between cation-anion pairs [31,34], obviating the need for analysis of individual atomic densities. Instead, a geometry-based method, which is the same for all semiconductors, is used to divide the volume of a tetrahedral multiatomic system into

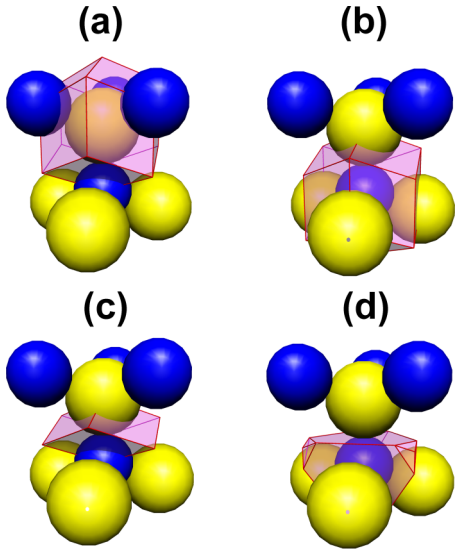

FIG. 3. Ball-and-stick models of the zinc-blende lattice, with cations and anions displayed in blue and yellow colors, respectively. (a) Anion-centered Wigner-Seitz (AWS) cell, (b) cation-centered Wigner-Seitz (CWS) cell, (c) quadrant, and (d) neutral polyhedron on the cation site.

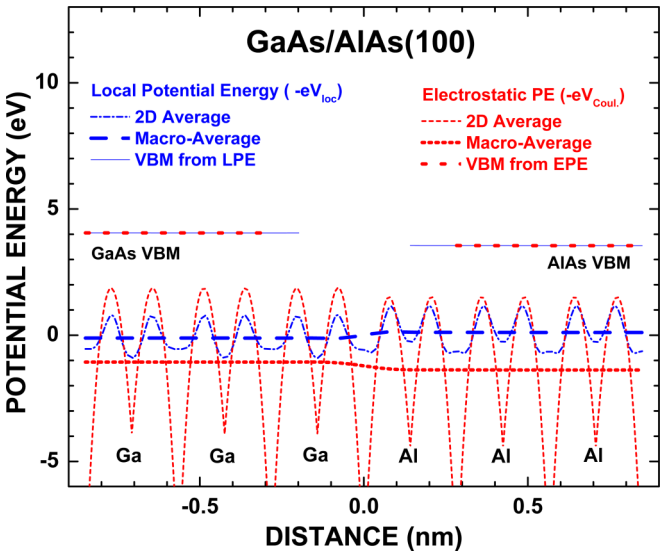

FIG. 4. Lateral two-dimensional (2D) average and macroscopic three-dimensional (3D) average of two types of potential energy, plotted along the length of a 12-layer GaAs/AlAs(100) supercell. The local potential energy ($-eV_{\rm loc}$) contains pseudopotential contributions. The electrostatic potential energy (EPE) ($-eV_{\rm Coul.}$) is the electrostatic (Coulomb) potential energy calculated from the pseudocharge density output. In the GaAs region of the supercell (left), the VBM position is computed and shown as a thin solid line, using the average $-e\overline{V_{\rm loc}}$ in this region and the known difference VBM $-e\overline{V_{\rm loc}}$ for bulk GaAs. Independently, the VBM in the GaAs region is also determined and shown as a coarse dotted line, using the average EPE ($-e\overline{V_{\rm Coul.}}$) in this region and relative position established for bulk GaAs. Similarly, the VBM is determined for the AlAs region (right) of the supercell with both methods, using relative positions established for bulk AlAs. Both methods yield indistinguishable VBM positions.

subvolumes, or quadrants, associated with each individual bond. To proceed, we note that the entire volume of a ZB crystal can be filled by placing Wigner-Seitz (WS) cells about each anion position, as shown in Fig. 3(a). An anion-centered WS (AWS) cell has a quarter (¼) cation at four of the eight threefold corners for a total of one full cation-anion pair in the cell. Alternatively, cation-centered WS (CWS) cells also fill the entire volume, as shown in Fig. 3(b). Because atom-centered WS cells (AWS and CWS) have vanishing net charge, dipole moment, and quadrupole moment, they are convenient building blocks for the construction of model solids with well-defined average internal potential energy and band edge positions, relative to an external vacuum level, as previously pointed out [20,43]. The overlapping volume between a pair of neighboring CWS and AWS cells, drawn in Fig. 3(c), contains ¼ anion, ¼ cation, and two valence electrons. It is defined here as a quadrant that houses the bond between this cation-anion pair. While such a volume may not contain the entirety of charge density associated with a bond within some definitions, nor is it devoid of charge density due to other bonds, its main character should reflect that of one bond. The validity of such an approximation, although anticipated from TB and DFT considerations, is only borne out in actual computations. There are four quadrants, oriented in different tetrahedral directions, in each AWS or CWS. Importantly, a semi-infinite sheet of quadrants has no net charge but has a net dipole moment that results in a definitive rise/drop in potential energy across the sheet. Quadrants are thus convenient units/components for potential analysis, as their electrostatic effects on the overall BO are well defined.

III. COMMON-ANION LATTICE-MATCHED HETEROJUNCTIONS

Three heterojunctions stand out as being nearly perfectly lattice-matched heterojunction systems, where the two semiconductors share a common anion. One, which is perhaps the most extensively studied semiconductor heterojunction with many practical applications, is the GaAs/AlAs junction [5,20,44–47]. The other two are GaP/AlP [48,49] and GaSb/AlSb [50–53]. We therefore begin with a detailed analysis of the GaAs/AlAs system, along all three major interface orientations—(100), (110) and (111)—and address the other two systems at the end of this section. Throughout this section, the very small lattice relaxations are found to have little effect on the magnitude of the VBO and are ignored in the calculations.

The plane-averaged local potential energy, $-eV_{\rm loc}$, obtained from a GaAs/AlAs(100) heterojunction, is plotted in the direction perpendicular to the heterojunction plane as a dash-dotted line in Fig. 4. Its macroscopically averaged [54] value, $-e\overline{V_{\rm loc}}$, i.e., its running average within a lattice-parameter-sized window along the plotted direction, is also shown as a thick dashed line, exhibiting a difference across the interface of 0.22 eV. The differences between the VBM and $-e\overline{V_{\rm loc}}$ on either side of the heterojunction, obtained from separate bulk calculations of GaAs and AlAs, are used to mark the VBM positions in Fig. 4 as thin solid lines. Using Eq. (1), these result in a VBO of 0.49 eV, in good agreement with experimental

results [45–47]. In this paper, a positive VBO indicates that the first semiconductor (e.g., GaAs) has a higher VBM than the second semiconductor (e.g., AlAs).

While $-e\overline{V_{\rm loc}}$ of the supercell and the bulk semiconductors is convenient for an accurate extraction of the theoretically predicted VBO for the heterojunction, it is not ideally suited for a detailed charge density analysis because it contains components of the pseudopotentials used in its calculation. To facilitate a comprehensive discussion of the relationship between BO and the interface charge distribution, purely electrostatic (Coulomb) potential energy distributions are generated for all the supercells, bulk semiconductors, and oligo-cells employed in the present paper. This is obtained for each system by adding suitably positioned point charges representing the pseudo-ion cores, e.g., +3e and +5e for Ga and As, respectively, to the electronic density distribution obtained from the first-principles calculation, resulting in a total charge distribution that is overall neutral. While this density is still affected by the pseudopotential, being a pseudo-density corresponding to valence electrons only, the ensuing electrostatic profile does not contain pseudopotential contributions directly. The resulting laterally averaged electrostatic potential energy, $-eV_{\rm Coul.}$, as well as its macroscopic average, $-e\overline{V_{\rm Coul.}}$, are also plotted in Fig. 4. As is well known [55], the absolute value of either $-eV_{\rm Coul.}$ or $-eV_{\rm loc}$ has no physical significance for a periodic system and therefore can be specified only to within an additive constant. For the same cell, however, these two quantities can only be subject to one arbitrary constant. A definitive offset between $-e\overline{V_{\rm Coul.}}$ and $-e\overline{V_{\rm loc}}$ has been established for every bulk semiconductor and for all pseudopotentials used in this paper by equating values in the interstitial part of the ZB unit cell, which is known to be free of pseudopotential contributions [56]. Plots of the electrostatic potential energy variation across a heterojunction, also in Fig. 4, confirm that the shifts between $-e\overline{V_{\rm Coul.}}$ and $-e\overline{V_{\rm loc}}$, as determined from separate bulk semiconductor calculations, are self-consistent. As shown in Fig. 4, the difference between the VBMs extracted from $-e\overline{V_{\rm Coul.}}$ and $-e\overline{V_{\rm loc}}$ is < 0.3 meV, on either side of the heterojunction. Being easier to modify in response to charge density changes, the electrostatic potential energy is considered henceforth. The differences between the VBM and the average electrostatic potential energy for all bulk semiconductors are given in Table I. The VBM positions obtained for various model solids of bulk semiconductor, with respect to vacuum level, are also listed in Table I. They are of general validity for interface analyses, even though pseudopotentials have been used in their calculations. The inclusion of core electrons in the calculation would have necessitated rigid shifts in the VBMs of model solids in Table I, but the VBO predicted using Table I would not have been affected.

The lateral average of the valence electron density that minimizes the energy for the GaAs/AlAs(100) supercell, as obtained from the DFT calculation, is shown as (i) of Fig. 5(a). The arrangement of atoms at this heterojunction is identical to that encountered in bulk GaAs on one side of the common As

TABLE I. Valence band maximum (eV) for various neutral model solids with respect to the vacuum level, calculated from the charge density of bulk semiconductors. Model solids CWS and AWS are constructed from charge densities of the respective WS cells. Cation plane (100) is a model solid terminated in the (100) direction on the plane of cations. The model solids for midplane (110) and neutral point (111) end on those two locations. The last column is the difference between the VBM and the average electrostatic (Coulomb) potential energy (EPE) of the model solid, which may be used to retrieve the average potential energy of each model solid. For example, the average electrostatic potential energy of a model solid constructed with anion Wigner-Seitz (AWS) cells of GaN is 10.979–6.455 = 4.524 eV.

Semiconductor	Lattice Constant (nm)	CWS	AWS	Cation Plane (100)	Anion Plane (100)	Mid-Pln (110)	Neutral Pt. (111)	VBM - Avg EPE
GaN	0.452	9.471	10.979	12.922	13.047	0.889	− 2.116	6.455
BP	0.452	17.970	8.223	11.152	21.354	2.796	− 0.723	9.436
AlP	0.545	10.034	6.712	8.571	13.063	− 0.300	− 2.775	5.138
GaP	0.545	10.517	6.586	8.510	13.408	− 0.134	− 2.475	5.274
AlAs	0.566	9.957	6.154	7.982	12.858	− 0.365	− 2.719	4.925
GaAs	0.566	10.490	6.083	7.967	13.261	− 0.132	− 2.364	5.116
InP	0.587	8.437	6.201	7.877	11.127	− 0.683	− 2.788	4.233
AlSb	0.609	10.343	5.187	7.012	13.003	− 0.197	− 2.475	4.870
GaSb	0.609	10.694	4.969	6.835	13.246	− 0.107	− 2.305	4.902
InAs	0.609	8.324	5.575	7.219	10.891	− 0.837	− 2.815	3.949
InSb	0.648	8.818	4.690	6.340	11.225	− 0.741	− 2.665	3.941
ZnS	0.545	10.773	16.531	20.142	13.882	− 1.591	− 3.676	5.877
BeTe	0.566	14.527	2.048	3.797	17.685	− 0.187	− 2.831	5.227
MgS	0.566	8.801	2.229	3.307	11.879	− 2.564	− 4.422	2.185
ZnSe	0.566	11.368	15.323	18.832	14.411	− 1.262	− 3.361	5.969
CdS	0.587	8.501	17.578	21.196	11.329	− 2.059	− 3.978	5.452
ZnTe	0.609	11.899	12.966	16.241	14.777	− 0.999	− 3.156	5.751
CdSe	0.609	8.998	16.227	19.714	11.763	− 1.906	− 3.762	5.357
CdTe	0.648	9.828	14.124	17.407	12.492	− 1.627	− 3.485	5.263
Si	0.545	9.385	9.385	11.867	11.867	0.613	− 1.968	6.179
Ge	0.566	9.045	9.045	11.412	11.412	0.607	− 1.721	5.916

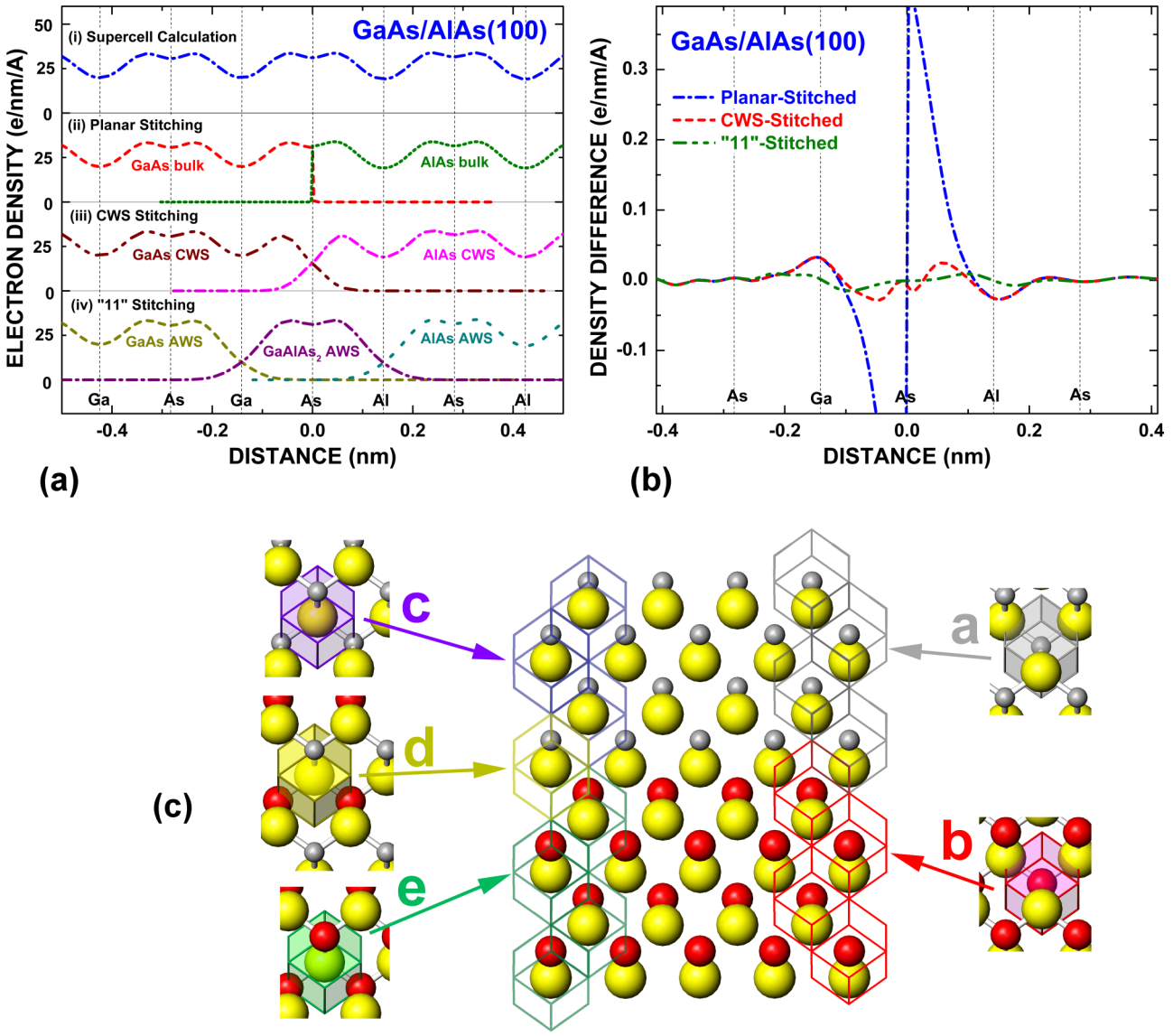

FIG. 5. (a) Electron density, per nm and per area of the two-dimensional (2D) unit cell (0.16 nm^2), of a GaAs/AlAs(100) supercell. (i) Obtained by *ab initio* calculation; (ii) from stitching bulk GaAs and bulk AlAs densities at the interface As plane; (iii) from stitching bulk GaAs and AlAs densities terminated at CWS boundaries; and (iv) from stitching the bulk GaAs AWS density, the bulk AlAs AWS density, and the density of an AWS cell from a "1 1" $GaAlAs_2$(100) cell (see text for details). (b) Difference between the equilibrium electron density calculated for a GaAs/AlAs(100) supercell and that constructed for the heterojunction by the various stitching methods. (c) Schematic illustration of two stitching methods for the simulation of charge density at the GaAs/AlAs(100) heterojunction. The atomic arrangement of the heterojunction is drawn in the center diagram, with As shown as large spheres, Al as small spheres, and Ga as midsized spheres. In the CWS-stitching method shown on the right, the volume of the heterojunction is divided into CWSs, and the charge density is stacked CWS-by-CWS with charge densities calculated for "a" bulk AlAs and "b" bulk GaAs. In the "1 1"-stitching method shown on the left, the volume of the heterojunction is divided into AWSs, and the charge density is stacked AWS-by-AWS with charge densities calculated for "c" bulk AlAs and "e" bulk GaAs, except for sites of the interface As common to both semiconductors. On these interface sites, AWSs are filled with charge density calculated for "d" an $AlGaAs_2$ oligo-cell.

plane and is indistinguishable from that of bulk AlAs on the other side. As mentioned above, this fact has often prompted the comparison of the charge density on either side with that of the respective bulk semiconductor. A model of the interface charge density can be constructed accordingly, as shown in panel (ii) of Fig. 5(a), by placing the two calculated bulk densities on opposite sides of the center As plane common to both semiconductors. Because of the symmetry of the ZB structure, such planar stitching of the charge density preserves the overall neutrality of the interface. However, the charge density thus stitched deviates appreciably from that calculated for the supercell, as shown in Fig. 5(b). Still, this deviation is significant only in the immediate interface region, essentially between the Ga and Al planes closest to the interface. This happens to be the region where the local atomic structure, with As being bonded to Al and Ga at opposite ends, is dissimilar

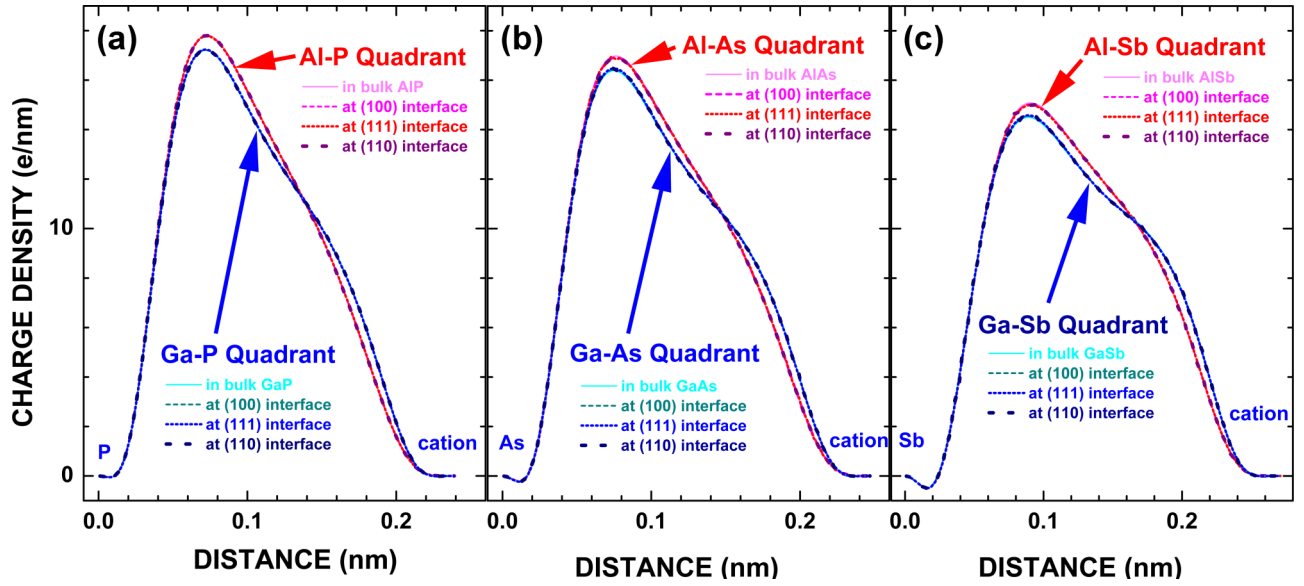

FIG. 6. Superimposed plots of charge density (per nm) of quadrants, integrated in the direction perpendicular to the center axis, ⟨111⟩, of Ga-anion and Al-anion quadrants, as extracted from the (100), (110), and (111) common anion III-V heterojunction interfaces, as well as from the bulk semiconductor. At the interfaces, the cation in the quadrant is bonded with both Ga and Al. (a) Ga-P and Al-P quadrants, (b) Ga-As and Al-As quadrants, and (c) Ga-Sb and Al-Sb quadrants.

to the structure encountered in either bulk AlAs or GaAs, from which the stitched density originates.

Planar stitching is chemically questionable because the charge distributions associated with individual bonds at the interface are not maintained as a unit. To correct for this shortcoming, the interface charge may be modeled by stitching together the bulk densities of GaAs and AlAs along boundaries between quadrants, thus approximately maintaining the integrity of the bulk bonds [20]. As shown in panel (iii) of Fig. 5(a) and on the right-hand half of Fig. 5(c), this is accomplished by summing the electron densities of the CWS for both bulk semiconductors. Doing so leads to a significant improvement over planar stitching in its ability to correctly model the equilibrium interface electron density, as shown in Fig. 5(b), and confirms the notion expressed earlier that the equilibrium charge distribution in ZB-based structures is analyzable, and approximately stackable, bond-by-bond (i.e., quadrant-by-quadrant). The close dependence of the electron distribution on the identities of the ions in the individual quadrant and the relative insensitivity of this charge density to the identities of second-nearest neighbors and beyond is further demonstrated in Fig. 6(b). It shows, as a function of the distance from the cation to the anion of a quadrant, the electron density integrated in the plane perpendicular to this direction. Clearly, this integrated electron density in a Ga-As quadrant is little changed from its bulk distribution when this quadrant is placed at GaAs/AlAs(100), (110), and (111) heterojunctions. At these heterojunctions, the As at the end of the quadrant forms bonds with 2Ga + 2Al, 1Ga + 3Al, or 3Ga + 1Al, respectively, while in bulk GaAs each As forms bonds with four Ga atoms. Correspondingly, Al-As quadrants also remain essentially bulklike when placed at these heterojunction interfaces, as also shown in Fig. 6(b).

It should be noted that such insensitivity of the quadrant charge distribution to its neighbors is only possible at neutral, e.g., isovalent, heterojunctions. At heterovalent interfaces, transfer of charge between neighbor quadrants may be appreciable [57]. Furthermore, because of the mismatches in the local electron density across boundaries between quadrants of different origins, some modification in the quadrant density is unavoidable if an equilibrium charge density for the heterojunction is to be reached. However, such modification may be kept to a minimum if the quadrants come from a chemical environment that reproduces the local arrangement of atoms to beyond the immediate cation-anion pair. Based on this insight, the CWS-stitched electron density for the GaAs/AlAs(100) interface, although already closely resembling the equilibrium supercell charge density, may be further improved. As shown on the left-hand side of Fig. 5(c), of the four quadrants associated with an interface As atom, the two on the GaAs side are from a chemical environment where every As ion has four Ga ions as nearest neighbors. At the CWS-stitched interface, they are stitched to Al-As quadrants, necessitating charge rearrangement before reaching equilibrium. A fix for this chemical mismatch, then, is to have the charge density near the interface As layer come from an environment where the As ion has two Al nearest neighbors and two Ga nearest neighbors. The smallest system one can construct in order to have such an atomic arrangement as part of its structure is a ternary $GaAlAs_2$ compound, marked "d" in Fig. 5(c), with alternating Ga and Al cation planes and with As occupying all anion positions. Here, we refer to such an oligo-cell as a one-one ("1 1") cell, as it consists of one full unit (chemical formula) each of the two semiconductors. Each having two bonds with Ga and two with Al, all As atoms in such a "1 1" cell are electrically equivalent. The AWS cells from the $GaAlAs_2$, based on the original (undoubled) ZB lattice, are therefore electrically neutral and may be used to make further adjustment in the stitched charge density of the GaAs/AlAs(100) interface. A layer of AWS of the "1 1" crystal may represent the

TABLE II. Valence band offset (VBO), in eV, calculated from first principles for three common-anion heterojunctions using heterojunction supercells with different orientations compared to VBOs modeled by stitching charge densities of bulk semiconductors and oligo-cells (see text and Figs. 5, 7, and 8 for details of the various stitching methods), experimental values, and VBO predictions from NPT.

Interface Orientation	Calculated/Modeled VBO (eV)	GaP/AlP	GaAs/AlAs	GaSb/AlSb
100	Supercell Calculation	0.439	0.507	0.321
	Anion Plane Stitched	0.345	0.403	0.244
	CWS Stitched	0.483	0.534	0.351
	"1 1" AWS Stitched	0.436	0.495	0.296
110	Supercell Calculation	0.436	0.497	0.326
	Mid-Plane Stitched	0.166	0.232	0.107
	CWS Stitched	0.483	0.534	0.370
	"1 1" Plane Stitched	0.395	0.457	0.304
	"2 2" Plane Stitched	0.438	0.511	0.343
111	Supercell Calculation	0.422	0.507	0.338
	Neutral Plane Stitched	0.300	0.355	0.170
	CWS Stitched	0.483	0.534	0.351
	Experiment[a]	0.43–0.57	0.42–0.55	0.39–0.45
	NPT w/correction	0.441	0.487	0.389
	NPT	0.303	0.357	0.259

[a]Refs. [44–48], [51–53].

charge density in the immediate interface region. Its LEGO is stitched to AWS-terminated charge density of the respective bulk semiconductor on either side, as shown in (iv) of Fig. 5(a) and on the left-hand side of Fig. 5(c). Because the charge densities of the "1 1" and GaAs now conjoin at a Ga site, there is no gross chemical mismatch that requires further attention. Similarly, chemical mismatch is also removed from the "1 1"-AlAs interface. Its every part being chemically similar to the corresponding part of supercell, the "1 1"-stitched charged density indeed closely resembles the supercell equilibrium density, as Fig. 5(b) reveals.

To estimate the VBO for the "1 1"-stitched heterojunction, one takes the difference between VBMs for AWS model solids listed in Table I, 6.083eV and 6.154 eV, respectively, for GaAs and AlAs, and subtracts the shift in average potential energy calculated for a layer of "1 1" AWS, −0.566 eV, to arrive at 0.495 eV. This and other VBOs deduced for differently stitched charge densities are listed in Table II. In line with the extent to which the density of each model deviates from the equilibrium density, the error made in predicting/reproducing the supercell VBO decreases from ∼0.1 eV for planar stitching, to ∼0.03–0.04 eV for CWS stitching, and to ∼0.01–0.02 eV eV for "1 1" stitching. It should be noted that in the literature, a 0.1 eV error in the VBO of a heterojunction is typically regarded as an excellent result for the model, as it is difficult to determine the VBO experimentally with an accuracy better than ∼0.1 eV [1].

We now turn to the (110) GaAs/AlAs heterojunction. The (110) planes in a ZB crystal are neutral, in the sense that each atomic plane contains equal densities of cations and anions. The analysis of the equilibrium charge density of the GaAs/AlAs(110) interface in terms of equilibrium densities for systems with similar local structures may therefore proceed, as for the (100) heterojunction, by stitching the GaAs and AlAs densities along planar and quadrant boundaries, as illustrated in Fig. 7. The midpoint between atomic planes is an appropriate location for planar stitching because the resulting stitched interface is assured of electrical neutrality. The average potential energy of bulk semiconductor crystals terminated on this plane can be found in Table I. Because a CWS-terminated (or AWS-terminated) ZB bulk crystal has an average potential energy that is related to the spherapole (trace of the density matrix) of the charge density and independent of the orientation of the surface [43], the CWS-stitched density must generate a VBO for the GaAs/AlAs(110) or the GaAs/AlAs(111) interface of exactly the same magnitude as that for the GaAs/AlAs(100) interface [20]. An examination of the CWS-stitched model finds each As atom on the interface GaAs plane to have been formed by joining three Ga-As quadrants and one Al-As quadrant. Similarly, each As atom on the interface AlAs plane has one Ga and three Al nearest neighbors. As discussed above, the minor charge rearrangement after CWS stitching may be largely accounted for by using LEGO with the exact local atomic arrangement. Incidentally, the "1 1" cell employed before for the (100) heterojunction may also be used here because such a cell, with alternating Ga and Al cation planes along one of the ⟨100⟩ directions, always has alternating GaAs and AlAs planes along two of its ⟨110⟩ directions, as "d" in Fig. 5(c) demonstrates. However, the use of a "1 1" cell, with As bonded to 2 Ga and 2 Al, does not completely remove the chemical mismatch from CWS stitching at the (110) interface. Nevertheless, as shown in Fig. 7(b), a significant improvement is already realized with "1 1" stitching. In general, quadrants from the "1 1" cell are not suitable for stitching as they may have a net charge. To satisfy the charge neutrality requirement, the location chosen for the stitching of the "1 1" cell is planar and on the atomic planes, as shown in Fig. 7(a).

To better match the chemical environment of the stitched structure to the actual atomic arrangement at the heterojunction interface, use may be made of oligo-cells with one or two more layers of atoms in the cell than in the "1 1" cell. All As atoms in a $GaAl_2As_3$ ("1 2") cell with its (110) planes repeated in the -GaAs-AlAs-AlAs- cycle and those in a Ga_2AlAs_3 ("2 1") cell

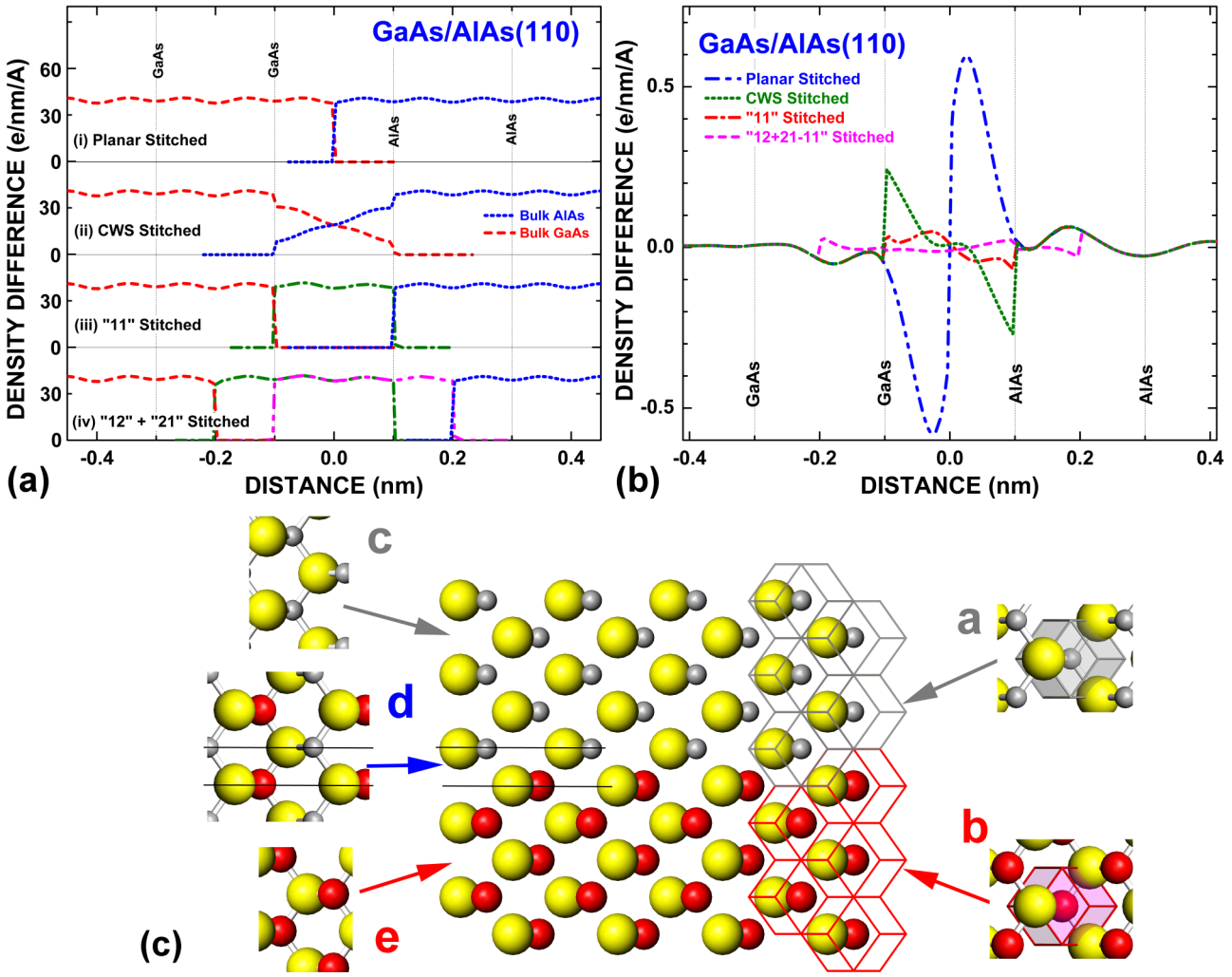

FIG. 7. (a) Electron density, per nm and per area of the two-dimensional (2D) unit cell (0.27 nm^2), of a GaAs/AlAs(110) supercell, obtained (i) by first-principles calculation; (ii) from stitching bulk GaAs and bulk AlAs densities on the midpoint between atomic planes; (iii) from stitching GaAs, AlAs, and "1 1" densities terminated on atomic planes; and (iv) from stitching GaAs, AlAs, "2 1" and "1 2" densities. (b) The difference (in e nm area) between the equilibrium electron density calculated for a GaAs/AlAs(110) supercell and that stitched together for this heterojunction with electron densities of bulk semiconductors and oligo-cells. (c) Schematic illustration of two stitching methods for the simulation of charge density at the AlAs/GaAs(110) heterojunction. The atomic arrangement of the heterojunction is drawn in the center diagram, with As, Al, and Ga shown, respectively, as large, small, and midsized spheres. In the CWS-stitching method shown on the right, the volume of the heterojunction is divided into CWSs, and the charge density is stacked CWS-by-CWS with charge densities calculated for "a" bulk AlAs and "b" bulk GaAs. In the "1 1"-stitching method shown on the left, the volume of the heterojunction is divided into three regions, by two parallel planes at locations of interface atoms. Charge densities calculated for "c" bulk AlAs and "e" bulk GaAs fill the outside regions, while the charge density from "d" an $AlGaAs_2$ oligo-cell fill the immediate interface region.

with –GaAs-GaAs-AlAs– stacking have mixed numbers of Ga and Al as nearest neighbors. By inserting the charge density from both the "2 1" cell and the "1 2" cell at the locations indicated in (iv) of Fig. 7(a), the charge density between the two immediate interface planes is doubly inserted. The redundant charge density in this region corresponds exactly to that of the "1 1" cell discussed earlier and shown in (iii) of Fig. 7(a). It may therefore be removed by a simple subtraction. It should be noted that these LEGOs being stitched/subtracted are all individually neutral. The resultant, "2 1" + "1 2" – "1 1" stitched, density is seen in Fig. 7(b) to closely approximate the equilibrium charge density of the supercell. The reason for such a stitching strategy is that all As atoms on the stitched interface GaAs plane come from a chemical environment with 3 Ga and 1 Al nearest neighbors and all As atoms on the interface AlAs plane have been calculated with 3 Al and 1 Ga as nearest neighbors, duplicating the chemical environment at the respective parts of the heterojunction. With the key to success identified as reproduction of the local chemical environment, it seems that an oligo-cell of $Ga_2Al_2As_4$, with its (110) planes repeating in a –GaAs-GaAs-AlAs-AlAs– cycle ("2 2"), could by itself reproduce the chemical environment of the (110) interface. This is found to be indeed the case. However, the "2 2" stitched results are not discussed further because they are nearly identical to results from "12 + 21 – 11"-stitched densities. The extent to which differently stitched (110) charge densities are able to quantitatively simulate the supercell VBO is further explored in Table II. It should be

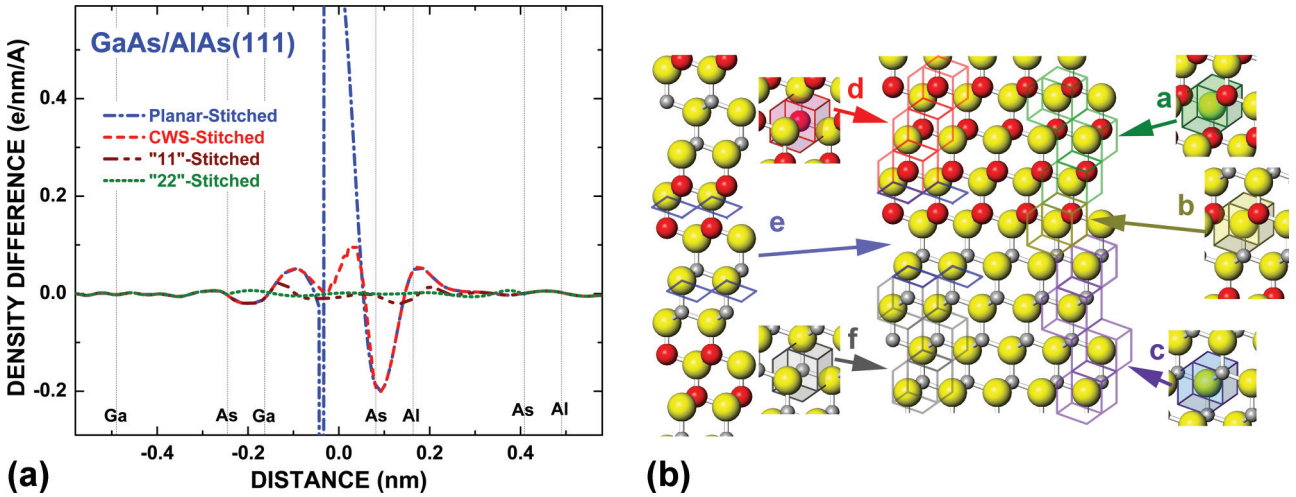

FIG. 8. (a) The difference (e per nm and per area) between the equilibrium electron density calculated for the GaAs/AlAs(111) supercell and that stitched together for this heterojunction with electron densities of bulk semiconductors and oligo-cells. (b) Schematic illustration of stitching methods for the simulation of charge density at the GaAs/AlAs(111) heterojunction. The atomic arrangement of the heterojunction is drawn in the center diagram, with As, Al, and Ga shown as large, small, and midsized spheres, respectively. In the "1 1"-stitching method shown on the right, the volume of the heterojunction is divided into AWSs, and the charge density is stacked AWS-by-AWS with charge densities calculated for bulk GaAs "a" and bulk AlAs "c," except for sites of the interface As common to both semiconductors. On those interface sites, AWSs are filled with charge density calculated for "b" the $AlGaAs_2$ oligo-cell. In the "2 2"-stitching method shown on the left, the volume of the heterojunction is divided into CWSs, and the charge density is stacked CWS-by-CWS with charge densities calculated for bulk GaAs "d" and bulk AlAs "f," except for cation sites closest to the interface. On those interface sites, charge density calculated for the $Al_2Ga_2As_4$ oligo-cell "e" is inserted.

clarified that the "1 2" and "2 1" cells just described are themselves one-half of a larger cell due to the constraint that the ZB (110) structure repeats in an even, not odd, number of atomic planes. Therefore, for example, the charge density used to fill the "1 2" position in Fig. 7(a) is actually that of one-quarter of a $Ga_2Al_4As_6$ cell. The use of a smaller but oblique oligo-cell is also possible here, although a larger cell is still preferred for the ability to place grid points (at which the density is sampled) at exactly the same positions in both the supercell and the oligo-cell.

There has not been much device work or research interest in (111)-oriented ZB heterojunctions. Scientifically, however, the formation of VBO at these heterojunctions must follow the same rules as for (100) or (110) oriented heterojunctions. Therefore, conclusions as to the charge distribution and BO formation at (111) heterojunctions carry as much importance and validity as those deduced for more frequently studied heterojunctions. Analysis of the electron distribution at the GaAs/AlAs(111) interface, however, requires more effort. The lack of a mirror plane or improper rotation (rotation-reflection) symmetry in the ZB (111) direction prevents the use of two electrically identical heterojunctions placed back-to-back in supercell or oligo-cell calculations. Any periodic-boundary calculation of the (111) heterojunction necessarily includes both (111)A and (111)B interfaces, with chemically similar atomic arrangements, at best, between the two semiconductors [58,59]. The two interfaces, although different in structural details, are presently found to be electrically similar for the GaAs/AlAs(111) supercell [20]. In constructing models of charge density for the heterojunction, the appropriate location for planar stitching is not known *a priori*. Of the two possible locations for a (111) planar termination that leave each semiconductor surface neutral, only the neutral point situated between bi-layers is chemically sensible. The neutral points for GaAs and AlAs happen to approximately coincide, allowing for planar stitching with negligible gap/overlap in the two bulk densities. The planar-stitched density, however, deviates considerably from the equilibrium heterojunction density, as shown in Fig. 8(a). Improvement can again be gained by CWS stitching, which works for the (111) interface without any neutrality concerns, as for other orientations. Further improvement is possible by noting that the chemical mismatch for the CWS-stitched density arises from the fact that the interface As is bonded to 3Al + 1Ga or 3Ga + 1Al, depending on whether the (111)A or the (111)B interface is being examined. Both atomic arrangements can be recreated in a "1 1" oligo-cell with alternating Al and Ga planes along the ⟨111⟩ direction, as schematically illustrated by "b" in Fig. 8(b). The charge in a layer of AWS cells, centered about As in the "1 1" cell with the corresponding local arrangement, can now be used and stitched with AWS densities from bulk GaAs and AlAs, as shown on the right-hand side of Fig. 8(b). Doing so indeed removes much of the chemical mismatch discrepancy, as shown in Fig. 8(a). It should be noted, however, that the "1 1" LEGO stitching just described is for reference and examination only. Because such an AWS cell is not, in general, electrically neutral, it is not physically meaningful to use the density so stitched for potential and VBO simulation. To model the potential distribution of the GaAs/AlAs(111) supercell without an obvious chemical mismatch, one can resort to a more conservative stitching scheme. Each half of a "2 2" oligo-cell in the ⟨111⟩ direction, marked by "e" in Fig. 8(b), contains the atomic arrangement found at either the (111)A or the (111)B interface, and each half is found to be approximately

neutral. Therefore, the half of the "2 2" cell corresponding to the GaAs/AlAs(111) interface being analyzed can be used, along with bulk densities, to create a "2 2" LEGO-stitched density, as shown on the left side of Fig. 8(b). Such a density not only closely reproduces the equilibrium charge density of the supercell, as shown in Fig. 8(a), but also approximately reproduces the VBO calculated with the supercell. Because the ZB structure repeats in the ⟨111⟩ direction every six atomic planes (three bi-layers), it should be noted that the densities for the "1 1" and "2 2" oligo-cells just described actually come from larger $(Ga_1Al_1As_2)_3$ and $(Ga_2Al_2As_4)_3$ cells, respectively.

Having examined the GaAs/AlAs heterojunction in detail, we turn to the other two lattice-matched common-anion heterojunctions, GaP/AlP and GaSb/AlSb. These have been studied along all three major interface orientations and in as much detail as just described for the GaAs/AlAs system. As shown in Fig. 6, the dependence of the local charge density on the local atomic structure, as well as the insensitivity of the local density to its neighbors, are exhibited in these systems as well. Therefore, the main results and conclusions pertaining to these systems are nearly identical to those presented for the GaAs/AlAs in Figs. 4–8 and are not described individually. Average potential energy and VBM positions for various surfaces of these semiconductors are given in Table I. The calculated VBOs of these heterojunctions, including those obtained from stitching, are shown in Table II and are also in good agreement with experiment [48,49,51–53]. To summarize, one notices the following: (1) the VBO is nearly independent of the orientation of the heterojunction; (2) the charge density at any part (quadrant) of an interface is dominated by the identities of the cation-anion pair of the quadrant; and (3) the potential distribution and the VBO of a heterojunction interface may be reproduced to within ∼0.04 eV by stitching bulk densities together along quadrant boundaries (CWS stitching). Correcting for chemical mismatches in the CWS-stitched density through the use of oligo-cell(s) further improves the agreement with the supercell charge density and potential energy distribution. One notes that since the equilibrium charge density of these supercells is found to be approximately a juxtaposition of quadrants of bulk densities (points 2 and 3 above), the relative insensitivity of the heterojunction VBO to the interface orientation (point 1 above) follows naturally.

IV. UNRELAXED ISOVALENT LATTICE-MATCHED HETEROJUNCTIONS

There are several lattice-matched, isovalent, ZB heterojunctions that share neither a common anion nor a common cation. As a result, at least two important features different from those of the heterojunctions discussed in the previous section emerge. First, there are at least two inequivalent interface bonding arrangements for each polar interface, i.e., (100) and (111), with possibly different VBOs [60–62]. Second, due to the presence of bonds at the interface that are different from that encountered in either semiconductor, interface relaxation is generally unavoidable for these heterojunctions in equilibrium [63]. The formation of the ground-state electron density for a particular atomic structure of the interface and the relaxation of atomic structure at the interface are, obviously, driven by minimization of the total interface energy. With these two processes intertwined at a relaxed heterojunction interface, the resulting electron density at the interface may be difficult to construct from densities of bulk semiconductors and small oligo-cells. Two approaches may be undertaken, then, to understand the equilibrium charge density at relaxed isovalent heterojunction interfaces. One is to monitor the formation of charge density in two steps: (a) the formation of unrelaxed heterojunction with the same atomic stacking as the eventual interface, followed by (b) the relaxation of the interface structure. Another is to directly compare the charge density of the relaxed heterojunction with that of a larger oligo-cell that encompasses the relaxed structure. Both approaches are taken in the present paper, so as to gain a fuller view of the chemistry at such interfaces and its relation to the BO.

In this section, we consider such junctions without lattice relaxation. In this case, the directions of all interface bonds are the same as in the bulk. One may then expect to model the charge distribution using bulk semiconductors and oligo-cells, as demonstrated above. As an illustrative example, we consider the InAs/GaSb(100) interface [64,65] with unrelaxed As-Ga interface bonds, shown schematically in Fig. 9. It may be viewed approximately as having been put together with an InAs bulk density (InAs CWS), a GaSb bulk density (GaSb AWS), and the density corresponding to As-Ga bonds (As-Ga quadrants). The last contribution may be extracted from a bulk GaAs crystal, calculated with the lattice parameter of the unrelaxed heterojunction. The use of an interface-specific cell, the As-Ga quadrant, not found in either bulk semiconductor, is reminiscent of the interface phase previously discussed as controlling the Schottky barrier height at oxide interfaces [66], although ZB is the only crystalline phase throughout the entire interface in the present paper. We refer to the density stitched together in this fashion, shown as (i) in Fig. 9(a), as single-layer quadrants (1Q) stitching. It approximately reproduces the equilibrium density obtained in supercell calculation, as shown in Fig. 9(b), but the fit is less than impressive. For many heterojunctions of this kind, summarized in Table III, the VBOs modeled by 1Q-stitching are not too far off from supercell values, but with some exceptions.

Examination of the charge density stitched together at this preliminary stage reveals chemical mismatches at both As and Ga locations at the immediate interface planes. The discussion of the previous section suggests that for the As atoms this may be remedied by using LEGO with an identical chemical environment, namely an $InGaAs_2$ "1 1" cell. Similarly, to correct for the chemical mismatch around the interface Ga atoms, a Ga_2AsSb "1 1" LEGO may be used. Taking both corrections is equivalent to stitching the densities of InAs(AWS), "1 1" InAs-GaAs, "1 1" GaAs-GaSb, and GaSb(CWS) together, as illustrated in Fig. 9. The charge density of a layer of As-Ga quadrants, which is double-counted in the process, is then subtracted to complete the "1 1 + 1 1 − 1Q" stitching. As shown in Fig. 9, such a LEGO-stitching strategy puts together a density that is very close to the equilibrium charge density of the supercell. The success of LEGO stitching in reproducing the VBOs obtained by supercell calculations has been observed in all of the unrelaxed, lattice-matched (100) heterojunctions presently studied, details of which can be found in Table III.

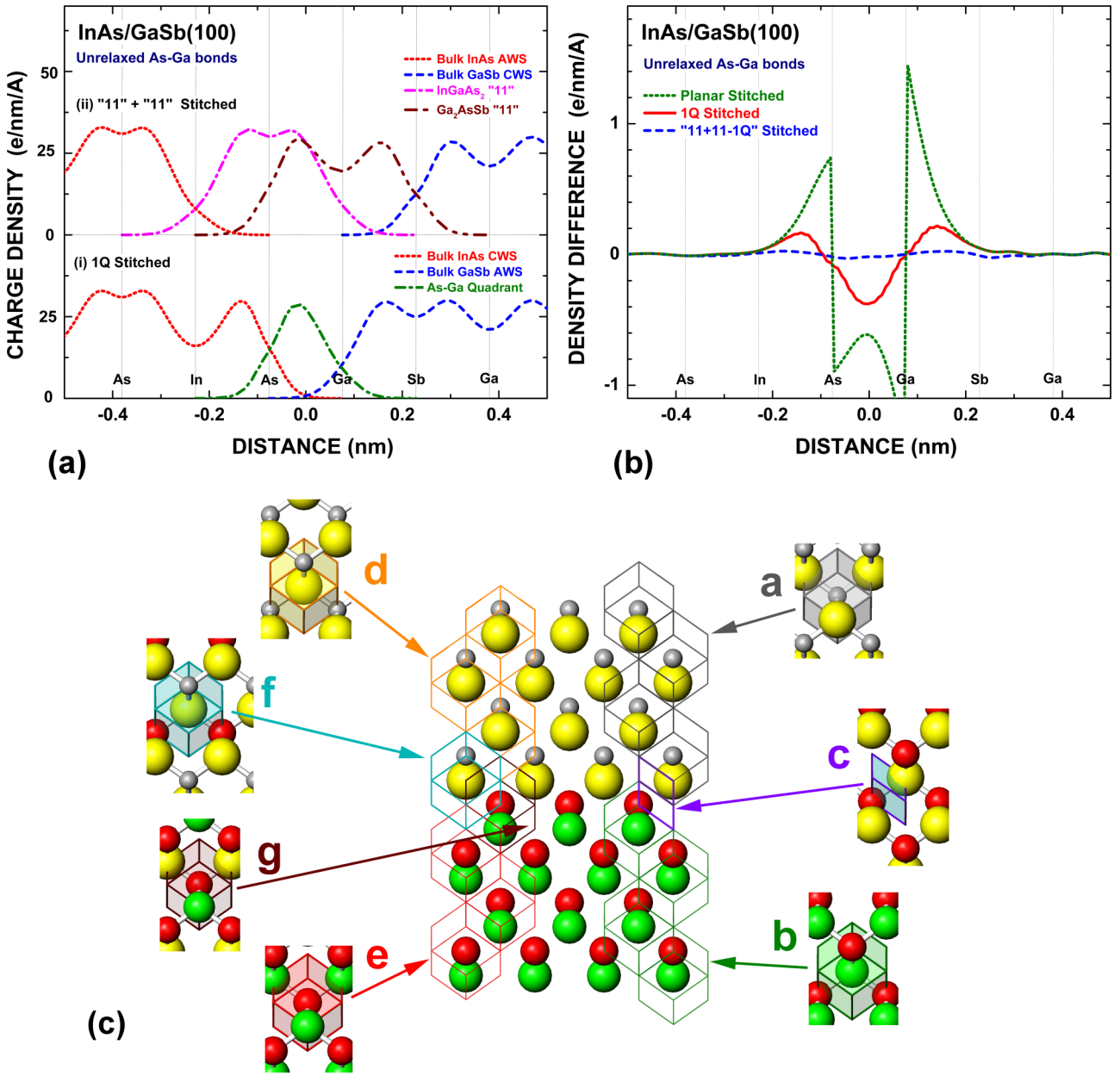

FIG. 9. (a) Electron densities, per nm and per area of the two-dimensional (2D) unit cell (0.185 nm^2), of bulk semiconductors and oligo-cells that are stitched together to simulate the charge density at the InAs/GaSb(100) heterojunction with As-Ga interface bonds. (b) The difference between the equilibrium charge density calculated for the unrelaxed InAs/GaSb(100) supercell with As-Ga interface bonds and the simulated LEGO-stitched charge density for this heterojunction, based on two stitching methods. (c) Schematic illustration of two stitching methods for the simulation of charge density at the (100) heterojunction between InAs (upper) and GaSb (lower), with As-Ga bonds. The atomic arrangement of the heterojunction is drawn in the center diagram, with anions shown as larger spheres and cations shown as smaller spheres. In the 1Q-stitching method shown on the right, the charge of the heterojunction is stacked together with "a" In-centered CWSs extracted from bulk InAs and "b" Sb-centered AWSs extracted from bulk GaSb. The gap at the interface is filled with "c" As-Ga quadrants extracted from a binary GaAs calculation. In the "11 + 11 − 1Q"-stitching method shown on the left, the charge density of the heterojunction, except at the immediate interface, is stacked together with "d" As-centered AWSs extracted from bulk InAs and "e" Ga-centered CWSs extracted from bulk GaSb. The interface region is filled with "f" As-centered AWSs from an $InGaAs_2$ "1 1" cell and "g" Ga-centered CWSs from a Ga_2InAs "1 1" cell. As drawn, the "1 1 + 1 1" -stitched density has overlaps in the interface As-Ga bond region. The charge density of a layer of "c" As-Ga quadrants is therefore removed to complete the "1 1 + 1 1 − 1Q" stitching on left.

For completeness, further types of stitching and heterojunctions are also studied in Table III. Results of stitching with an appropriate "1.5 1.5" oligo-cell, e.g., $InAs_2Ga_2Sb$ for the InAs/GaSb(100) with As-Ga bonds, are also found to be very satisfactory, as Table III reveals. We defer discussion of this stitching method to the discussion of relaxed interfaces below. Also included in Table III are some heterojunction interfaces with an interface atomic layer replaced by a layer

TABLE III. Computed valence band offsets (VBOs), in eV, of unrelaxed, isovalent, lattice-matched (100) heterojunctions. The type of interface bond is given in parentheses. Heterojunctions marked by three atomic layers, e.g., (Be-S-Zn), contain an atomic interlayer. The oligo-cells used for multiple LEGO stitching are listed on the last column. For interfaces without an interlayer, a single layer of quadrants (1Q) is used for stitching in the next to last column. For interfaces with interlayers, the "1 1" oligo-cell is used in that column. The "1.5 1.5" oligo-cell contains two additional planes of interlayer atoms.

Unrelaxed (100) Heterojunction	Supercell VBO (eV)	"1.5 1.5" Stitched	Multiple LEGO Stitched	1Q or "11" Stitched	Oligo-Cells Used
BP/GaN (P-Ga)	0.723	0.584	0.669	0.932	Ga_2PN, $BGaP_2$, GaP
BP/GaN (B-N)	0.605	0.700	0.711	0.209	B_2PN, $BGaN_2$, BN
BeTe/ZnSe (Be-Se)	0.078	0.085	0.091	0.224	Be_2TeSe, $BeZnSe_2$, BeSe
BeTe/ZnSe (Te-Zn)	0.127	0.181	0.220	0.438	Zn_2TeSe, $BeZnTe_2$, ZnTe
BeTe/ZnSe (Be-S-Zn)	0.046	0.020	0.013	0.342	Be_2TeS, Zn_2SSe, $BeZnS_2$, BeS, ZnS
BeTe/ZnSe (Te-Cd-Se)	0.228	0.240	0.373	0.083	$BeCdTe_2$, $CdZnSe_2$, Cd_2TeSe, CdTe, CdSe
BeTe/ZnSe (Te-Mg-Se)	0.233	0.201	0.181	0.071	$BeMgTe_2$, $MgZnSe_2$, Mg_2TeSe, MgTe, MgSe
BeTe/MgS (Be-S)	1.093	1.124	1.160	1.202	Be_2TeS, $BeMgS_2$, BeS
BeTe/MgS (Te-Mg)	1.345	1.313	1.336	1.537	Mg_2TeS, $BeMgTe_2$, MgTe
BeTe/MgS (Be-Se-Mg)	1.202	1.179	1.253	1.808	Be_2TeSe, Mg_2SeS, $BeMgSe_2$, BeSe, MgSe
BeTe/MgS (Te-Zn-S)	1.188	1.215	1.359	0.792	$BeZnTe_2$, $ZnMgS_2$, Zn_2TeS, ZnTe, ZnS
MgS/ZnSe (Mg-Se)	− 1.095	− 1.129	− 1.155	− 1.097	Mg_2SSe, $MgZnSe_2$, MgSe
MgS/ZnSe (S-Zn)	− 1.028	− 1.082	− 1.139	− 1.087	Zn_2SSe, $MgZnS_2$, ZnS
MgS/ZnSe (Mg-Te-Zn)	− 1.172	− 1.082	− 1.104	− 1.161	Mg_2STe, Zn_2TeSe, $MgZnTe_2$, MgTe, ZnTe
MgS/ZnSe (S-Be-Se)	− 0.995	− 1.040	− 1.073	− 0.787	$MgBeS_2$, $BeZnSe_2$, Be_2SSe, BeS, BeSe
MgSe/CdS (Mg-S)	− 0.692	− 0.705	− 0.722	− 0.537	$SeSMg_2$, $MgCdS_2$, MgS
MgSe/CdS (Se-Cd)	− 0.696	− 0.662	− 0.664	− 0.497	$MgCdSe_2$,SeS Cd_2, CdSe
InAs/AlSb (In-Sb)	0.099	0.045	0.058	− 0.0699	In_2AsSb, $InAlSb_2$, InSb
InAs/AlSb (As-Al)	0.087	0.037	0.047	− 0.0172	Al_2AsSb, $InAlAs_2$, AlAs
InAs/AlSb (As-Ga-Sb)	0.122	0.050	0.087	0.384	$InGaAs_2$, $AlGaSb_2$, Ga_2AsSb, GaAs, GaSb
InAs/AlSb (In-P-Al)	0.086	0.053	0.060	− 0.242	In_2AsP, Al_2PSb, $InAlP_2$, InP, AlP
InAs/GaSb (In-Sb)	− 0.215	− 0.243	− 0.232	− 0.421	In_2AsSb, $InGaSb_2$, InSb
InAs/GaSb (As-Ga)	− 0.189	− 0.219	− 0.213	− 0.395	Ga_2AsSb, $InGaAs_2$, GaAs
InAs/GaSb (As-Al-Sb)	− 0.219	- − 0.274	− 0.248	− 0.034	$InAlAs_2$, $AlGaSb_2$, Al_2AsSb, AlAs, AlSb
InAs/GaSb (In-P-Ga)	− 0.175	− 0.207	− 0.187	− 0.630	In_2AsP, Ga_2PSb, $InGaP_2$, InP, GaP
ZnTe/CdSe (Zn-Se)	0.109	0.188	0.214	0.426	Zn_2TeSe, $ZnCdSe_2$, ZnSe
ZnTe/CdSe (Te-Cd)	0.184	0.285	0.326	0.496	Cd_2TeSe, $ZnCdTe_2$, CdTe
ZnTe/CdSe (Zn-S-Cd)	0.070	0.119	0.152	0.617	Zn_2TeS, Cd_2SSe, $ZnCdS_2$, ZnS, CdS

of isovalent atoms. For example, the interface Ga for the InAs/GaSb(100) heterojunction with As-Ga bonds may be replaced by a layer of Al, resulting in an interface with an –In–As-Al-Sb-Ga– stacking sequence. We refer to such an interface as an InAs/GaSb(100) heterojunction with an Al interlayer. The charge density at these heterojunctions may also be appropriately stitched together using the same rules on chemical adjustment as demonstrated in examples above, although more LEGOs are required for such interfaces. As can be seen from Table III, the use of isovalent interlayers, either cationic or anionic, does not strongly affect the VBO of the heterojunction.

We now turn to unrelaxed isovalent heterojunctions with (110) orientation. The most straightforward way to stitch the (110) heterojunction density is through planar stitching along the midpoint between atomic layers, as (i) of Fig. 7(a) suggests. However, this simple method leads to poor results due to disparity in the atomic arrangement, as shown in Fig. 10 for the unrelaxed BeTe/MgS(110) junction [4]. As also shown in Fig. 10, 1Q stitching provides for better agreement. In this case, it uses bulk densities of MgS and BeTe throughout, except for the quadrants across the immediate interface planes, for which the densities of bulk MgTe and BeS, calculated at the unrelaxed

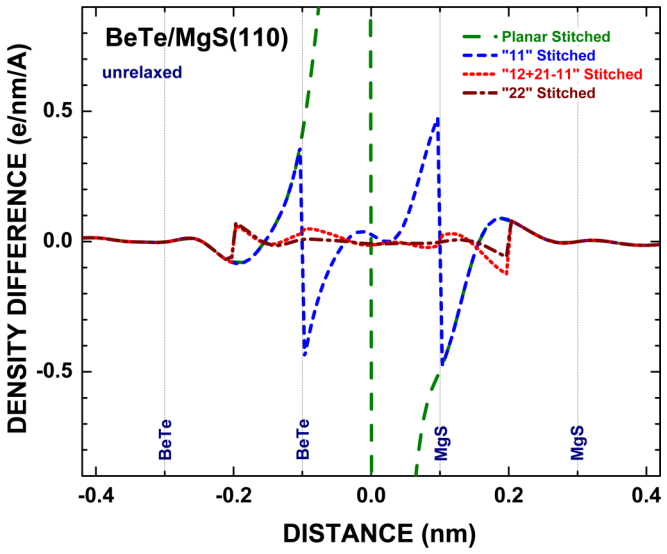

FIG. 10. The difference (in e nm area) between the equilibrium charge density calculated for an unrelaxed BeTe/MgS(110) supercell and the simulated charge density obtained for the same heterojunction from various stitching methods described in the text.

lattice constant of BeTe, are used. Geometrical analysis shows that stitching in this manner would produce a VBO that is the average of the VBOs produced by 1Q stitching for the two unrelaxed BeTe/MgS(100) interfaces, i.e., with Be-S and Mg-Te interface bonds. Without any chemical adjustment, 1Q stitching typically produces VBOs that are in acceptable, but not impressive, agreement with the calculated VBO for the supercell, ∼0.03–0.3 eV. Other methods of stitching for the (110) interface have already been described in detail and schematically shown in Fig. 7(a). With nearly complete removal of chemical mismatches, the "1 2 + 2 1–1 1"-stitching strategy best reproduces the equilibrium charge density of the BeTe/MgS(110), as shown in Fig. 10, as well as its VBO, as shown in Table IV. Examination of calculated VBOs for other (100) and (110) junctions in Tables III and IV, respectively, shows that the VBO for an unrelaxed heterojunction does not have a strong dependence on either the interface orientation or the identity of the interface bonds, e.g., the VBOs for InAs/GaSb(110) and InAs/GaSb(100) with As-Ga bond, and InAs/GaSb(100) with In-Sb bonds [62] are all similar. This insensitivity of the VBO to interface specifics is found to be in effect for all III-V and II-VI heterojunctions studied here.

Because even the modest and straightforward 1Q-stitching method renders a VBO that is largely independent of the interface orientation and the identity of the interface bonds, clearly this insensitivity is in force even without detailed chemical matching and therefore seems to point to some invariable characteristics of the charge distribution in bulk semiconductors. In 1Q stitching, charge density is made up exclusively of quadrants from bulk semiconductors. Therefore, this method can predict similar VBOs for the two possible (As-Al or In-Sb bonded) InAs/AlSb(100) heterojunctions only if the overall potential energy changes across a layer of As-Al quadrants plus a layer of Al-Sb quadrants, or across a layer of As-In quadrants plus a layer of In-Sb quadrants, is essentially the same. Naturally, all these quadrants are obtained from bulk semiconductor calculations, with the same 0.609-nm lattice constant that characterizes this epitaxial system. Potential energy changes so calculated, also for additional semiconductors assuming the same 0.609-nm lattice constant, are listed in Table V. The table confirms that indeed the two InAs/AlSb(100) bonding scenarios have nearly identical potential energy changes −2.00 eV and −1.95 eV (the difference between entries in the As and Sb rows for the Al and In columns), respectively—accounting for their similar VBOs. However, a far more striking feature of Table V is the fact that the difference in values between any two columns, or any two rows, is almost constant. In other words, switching the identity of the cation of the semiconductor, e.g., from Al to Ga, leads to approximately the same change in potential energy, regardless of the identity of the anion, and likewise for an anionic switch.

TABLE V. Potential energy drop (in eV) across a full layer of (cation to anion) quadrants of III-V semiconductors, with the cation and the anion arranged as column and row, respectively. All semiconductors are calculated with an assumed lattice constant of 0.609 nm.

Anion \ Cation	Al	Ga	In
P	−2.392	−2.994	−2.003
As	−3.154	−3.749	−2.748
Sb	−5.156	−5.725	−4.698

The above observation suggests that the total potential energy drop for a layer of semiconductor quadrants should be separable into two individual additive contributions, one from the cation and the other from the anion. To observe this, the laterally averaged potential energy distributions across the above III-V quadrants are shown in Fig. 11(a). Note that the potential energy remains constant to the left and to the right of the curves plotted. In the figure, the left (cation) ends of the quadrant curves are shifted vertically to reflect the differences between columns of Table V. This causes the right (anion) ends of the curves to converge closely into groups, ending with values that reflect the differences between rows of Table V. This separability, or additivity, of cation and anion contributions to the quadrant potential energy is not limited to III-V semiconductors, nor is it valid only for a particular lattice parameter. Figure 11(a) also features various II-VI quadrants, and Fig. 11(b) shows that the same is true for a different (0.566 nm) lattice constant. Clearly, many of the semiconductor combinations considered in Fig. 11 are artificial in that they have not been calculated at their natural lattice parameter. Nevertheless, the chemical trend displayed in Fig. 11 reflects the electronic density distribution that minimizes the total energy for the particular geometry chosen and therefore serves below as a valid and important aid to modeling the electrostatic effect associated with lattice relaxation. One more important

TABLE IV. Valence band offsets (VBOs), in eV, of unrelaxed, isovalent, lattice-matched (110) heterojunctions, computed from heterojunction supercells, compared with those computed from various stitching methods described in the text.

Unrelaxed (110) Heterojunction	Supercell	"22" Stitched	"12 + 21 − 11" Stitched	1Q Stitched	"11" Stitched
BP/GaN(110)	0.639	0.634	0.672	0.570	0.498
BP/AlN(110)	1.567	1.530	1.568	1.455	1.205
BeTe/ZnSe(110)	0.114	0.145	0.170	0.331	0.249
BeTe/MgS(110)	1.232	1.227	1.274	1.369	1.134
MgS/ZnSe(110)	− 1.063	− 1.103	− 1.137	− 1.092	− 0.961
MgSe/CdS(110)	− 0.689	− 0.664	− 0.664	− 0.517	− 0.513
InAs/AlSb(110)	0.078	0.069	0.062	− 0.044	− 0.036
InAs/GaSb(110)	− 0.139	− 0.237	− 0.236	− 0.408	− 0.341
ZnTe/CdSe(110)	0.165	0.262	0.287	0.461	0.359

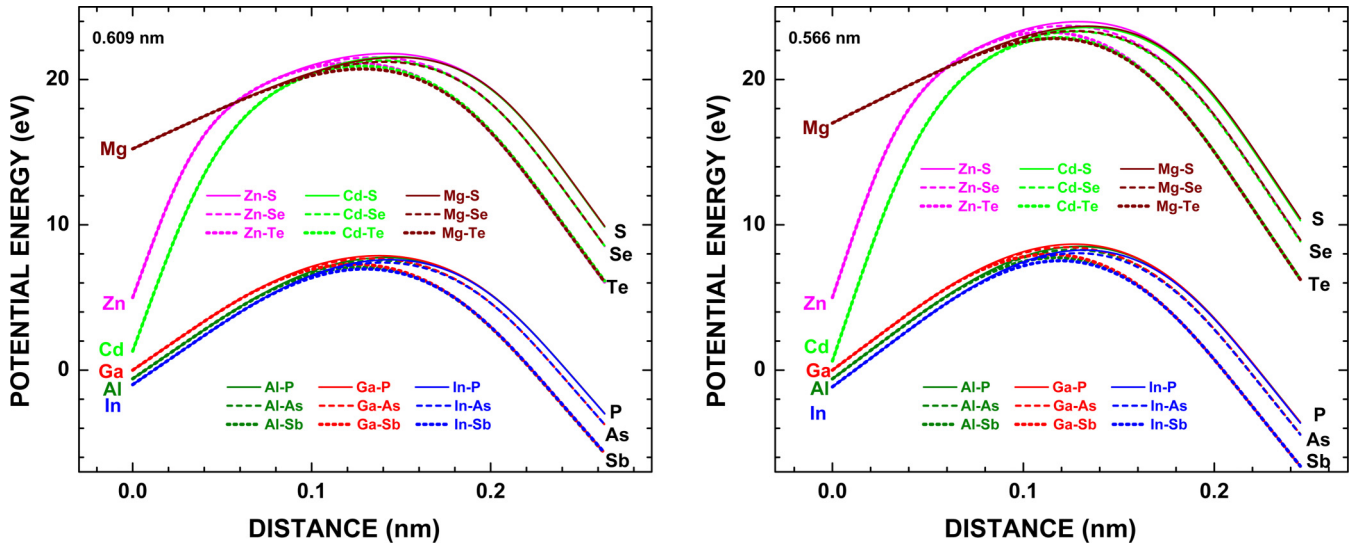

FIG. 11. (a) Laterally averaged electrostatic potential energy profile across a layer of quadrants of III-V semiconductors, calculated with a lattice constant of 0.609 nm. The quadrants are aligned in the ⟨111⟩ direction and have an areal density that is given for the zinc blende crystal by $(\sqrt{3}/4 \cdot a^2)^{-1} \sim 6.23\,\mathrm{nm}^{-2}$. The potential energy curves have been vertically shifted by amounts suggested in Table V. (b) Same as (a), except the calculations are done with a lattice constant of 0.566 nm and a corresponding areal density of $\sim 7.21\,\mathrm{nm}^{-2}$.

outcome of this apparent separability of potential energy is the approximate independence of the VBO for a heterojunction of not only the interface bonds and orientation but also the insertion of an isovalent interlayer at the heterojunction interface. It should be pointed out that even though Fig. 11 and Table V suggest the separability of cation and anion contributions in the potential energy of a quadrant, these plots do not point to a specific, physically motivated way to actually make such a separation. We shall return to this in the next section, but for now note that such quadrant partition is unnecessary for the analysis of unrelaxed interfaces.

V. RELAXED ISOVALENT LATTICE-MATCHED HETEROJUNCTIONS

We begin our investigation of the effect of lattice relaxation by considering (100) isovalent, lattice-matched heterojunctions, where the atomic positions for the interface planes are allowed to relax in the direction perpendicular to the interface. We use the relaxed BeTe/MgS(100) heterojunction as an illustrative example, with Be-S or Te-Mg interface bonds. For either, the positions of the two atomic layers involved in the interface bonds are relaxed, leading to changes in three interplanar distances. Upon relaxation, bonds associated with atoms on four atomic layers are distorted from their ideal tetrahedral network, making modeling of the charge density with that of perfectly tetrahedral oligo-cells questionable. We have seen repeatedly that the heterojunction electron density is governed predominantly by local atomic structure. It therefore stands to reason that the charge density calculated for oligo-cells with atomic relaxation identical to that found in the supercell may still offer useful information. For BeTe/MgS(100) heterojunction with relaxed Be-S bonds, the use of a "1.5 1.5" Be_2TeMgS_2 oligo-cell, consisting of back-to-back Te–Be(relaxed)–S(relaxed)–Mg planes, recreates the atomic arrangement in the most critical part of the heterojunction. The right-hand side of Fig. 12(c) demonstrates how the LEGO from such a "1.5 1.5" cell may be stitched with bulk densities on both sides. However, because of lattice relaxation, the "1.5 1.5" oligo-cell contains no atoms with bonds in perfect tetrahedral directions and therefore is always mismatched with the structure of bulk semiconductors when stitched. This is illustrated in Fig. 12(a), which shows that the equilibrium heterojunction density is approximately recreated by "1.5 1.5" stitching, but the agreement is less than perfect. A similar conclusion arises for the Te-Mg bonded interface in Fig. 12(b). The remaining discrepancies are likely due to bond-angle mismatches because for interfaces without lattice relaxation, discussed earlier and summarized in Table III, the same "1.5 1.5" stitching approach works very well indeed. By padding with two more atomic planes between interfaces, as shown on the left-hand side of Fig. 12(c), a $Be_3Te_2Mg_2S_3$ "2.5 2.5" oligo-cell is formed that correctly reproduces the entire atomic arrangement of the supercell (we note that for reasons related to the ZB structure already described above, the "1.5 1.5" and "2.5 2.5" cells are actually calculated with twice the intended cell length). With only one layer of undistorted tetrahedral bonds separating every four atomic layers with distorted bonds, such a "2.5 2.5" cell has the minimum number of atomic planes necessary to replicate the interface structure of the relaxed supercell. Not surprisingly, the charge density thus stitched is in very good agreement with that calculated for the BeTe/MgS(100) supercell with either Be-S or Te-Mg interface bonds, as shown in Figs. 12(a) and 12(b). The VBOs calculated for relaxed supercells, as shown in Table VI, are in excellent agreement with that modeled with "2.5 2.5" stitching. Interestingly, the "1.5 1.5" stitching method, even with its just-discussed problems, generally reproduces the VBO to ∼0.1 eV!

Turning to relaxed (110) heterojunctions, all atoms on the two immediate interface planes are allowed to relax in both in-plane and out-of-plane directions. Energy minimization

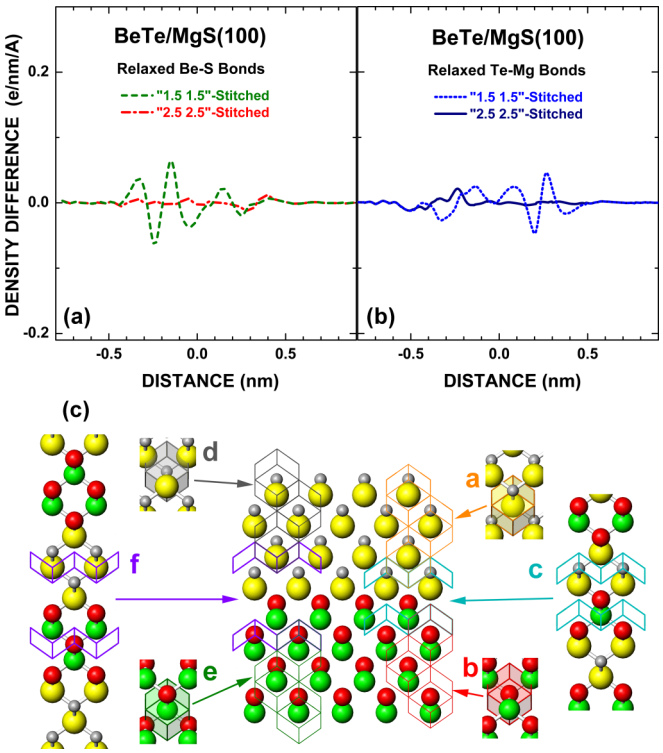

FIG. 12. Difference between the equilibrium charge density (in e per nm per area) calculated for a supercell and that stitched together with bulk and oligo-cell densities for the BeTe/MgS(100) heterojunction with (a) relaxed Be-S interface bonds and (b) relaxed Te-Mg interface bonds. There is an overall contraction between the two semiconductors of ∼0.031 nm for the Be-S bonded interface and an expansion of ∼0.042 nm for the Te-Mg bonded interface. (c) Schematic illustration of the two stitching methods for a heterojunction between BeTe (upper) and MgS (lower), with Te-Mg bonds. The atomic arrangement of the heterojunction is drawn in the center diagram, with anions shown as larger spheres and cations shown as smaller spheres. In the "1.5 1.5"-stitching method shown on the right, the charge of the heterojunction is stacked together with Be-centered CWSs extracted from bulk BeTe (upper right) and S-centered AWS extracted from bulk MgS (lower right). The gap at the interface is filled with density extracted from a $BeTe_2Mg_2S$ calculation (middle right). In the "2.5 2.5"-stitching method shown on the left, the charge density of the heterojunction is stacked together with Te-centered AWS's extracted from bulk BeTe and an Mg-centered CWS extracted from bulk MgS. The interface region is filled with charge density from a $Be_2Te_3Mg_3S_2$ calculation.

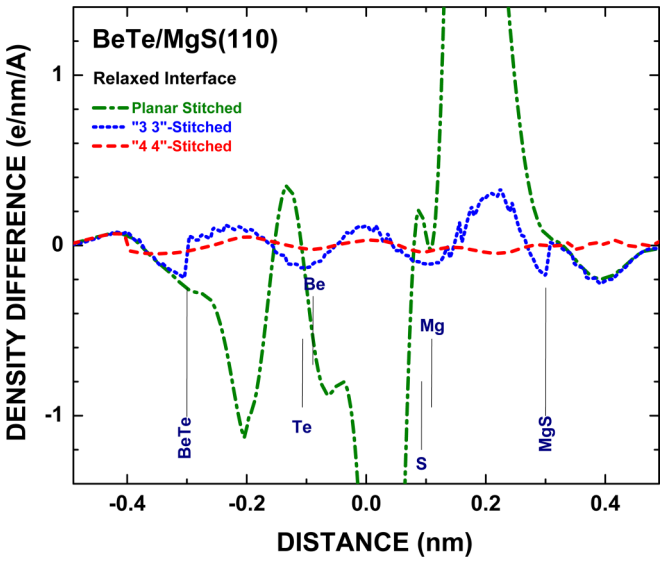

FIG. 13. Difference between the equilibrium charge density (in e per nm per area) calculated for supercell and that stitched together with bulk and oligo-cell densities for the relaxed BeTe/MgS(110) heterojunction. The locations of relaxed atoms are indicated. Additionally, atoms relax laterally, and there is a small overall expansion, ∼0.004 nm, between the two bulk crystals. The relaxed atomic structure for the supercell is also employed for the "3 3" and "4 4" oligo-cells.

frequently results in an expansion in the overall interface distance from the nominal bulk distance. With atomic positions relaxed, at least some of the bonds on four atomic layers at the interface are distorted from their tetrahedral orientations and/or length. For the example of the relaxed BeTe/MgS(110) heterojunction, the interface contains –BeTe–BeTe(relaxed)–MgS(relaxed)–MgS– planes, which can be arranged back-to-back to form a $Zn_3Te_3Cd_3Se_3$, "3 3" oligo-cell with exactly the same lattice relaxation as the heterojunction. However, such an oligo-cell contains no atoms with undistorted bonds and therefore always has disparate bond angles when stitched to the density of bulk semiconductors. Nevertheless, the equilibrium charge density of the heterojunction can be recreated reasonably, as shown in Fig. 13, and the VBO approximately modeled, as shown in Table VI, by "3 3" stitching. Adding one more unrelaxed layer of atoms between interfaces to the "3 3" cell creates a "4 4" $Zn_4Te_4Cd_4Se_4$ oligo-cell, whose density and VBO very well match that of the supercell, as also shown in Fig. 13 and Table VI. Note that despite the seemingly large number of atoms in the "4 4" oligo-cell, there is actually no atom in such a (110) oligo-cell with completely undistorted tetrahedral bonds! A summary of results of supercell calculation on relaxed heterojunctions and VBOs modeled by appropriately chosen oligo-cells can be found in Table VI.

The excellent agreement between the stitched charge density and the equilibrium supercell density for both (100) and (110) relaxed heterojunctions again marks the localness, or the nearsightedness [67], in the coupling between the charge density and the atomic structure, just as demonstrated in the previous section for unrelaxed heterojunctions. However, the relaxation is significant and plays an important role in the BO formation. For (100) heterojunctions between the same two semiconductors but with different interface bonds, lattice relaxations are generally found to be significantly different. For example, the As-Ga bonded interface of InAs/GaSb(100) has an overall contraction while the In-Sb bonded interface involves a significant overall expansion [64,65]. The directions of these atomic movements reflect the fact that the equilibrium As-Ga and In-Sb bonds are shorter and longer, respectively, than the bulk bond length in this epitaxial system. For the (110) junction between the same semiconductors, the cation and anion on one atomic plane have different in-plane and out-of-plane relaxations, resulting in different lengths for the

TABLE VI. Valence band offset (eV) of relaxed, isovalent, lattice-matched heterojunctions. For the (100)-heterojunctions, the type of interface bond is written in parentheses. The long and short LEGOs used for the stitching come, respectively, from "2.5 2.5" and "1.5 1.5" oligo-cells for (100) heterojunctions. For (110) heterojunctions, these come respectively from "4 4" and "3 3" oligo-cells. The predictions from NPT and NPT with correction are shown. Also shown as footnotes are experimental VBOs, where available.

Relaxed Heterojunction Interface	Supercell VBO (eV)	Long LEGO Stitched	Short LEGO Stitched	NPT with corrections	Neutral Polyhedron Theory
PB/GaN(100) (P-Ga)	1.406	1.537	0.996	1.308	1.420
PB/GaN(100) (B-N)	1.453	1.475	1.574		
BP/GaN(110)	1.728	1.703	1.817		
MgSe/CdS(100) (Mg-S)	− 0.238	− 0.241	− 0.126	− 0.093	− 0.142
MgSe/CdS(100) (Se-Cd)	− 0.541	− 0.560	− 0.617		
MgSe/CdS(110)	− 0.368	− 0.342	− 0.276		
BeTe/ZnSe(100) (Be-Se)	0.532	0.528	0.469	0.635	0.503
BeTe/ZnSe(100) (Zn-Te)	0.443	0.433	0.316		
BeTe/ZnSe(110)	0.530	0.572	0.502		
BeTe/MgS(100) (Be-S)	1.863	1.880	1.905	1.697	1.568
BeTe/MgS(100) (Te-Mg)	2.145	2.176	2.050		
BeTe/MgS(110)	2.196	2.264	2.338		
MgS/ZnSe(100) (S-Zn)	− 1.338	− 1.344	− 1.451	− 1.062	− 1.065
MgS/ZnSe(100) (Mg-Se)	− 1.305	− 1.307	− 1.389		
MgS/ZnSe(110)	− 1.409	− 1.420	− 1.572		
InAs/AlSb(100) (In-Sb)	− 0.074	− 0.125	− 0.039	− 0.202	− 0.339
InAs/AlSb(100) (As-Al)	− 0.188	− 0.288	− 0.416		
InAs/AlSb(110)	− 0.206	− 0.194	− 0.301		
InAs/GaSb(100) (As-Ga)[a]	− 0.380	− 0.469	− 0.543	− 0.482	− 0.507
InAs/GaSb(100) (In-Sb)	− 0.360	− 0.375	− 0.379		
InAs/GaSb(110)	− 0.427	− 0.420	− 0.405		
ZnTe/CdSe(100) (Zn-Se)[b]	0.533	0.572	0.644	0.579	0.601
ZnTe/CdSe(100) (Te-Cd)	0.412	0.440	0.430		
ZnTe/CdSe(110)	0.521	0.527	0.625		

[a]Experiment: $-0.51 \sim -0.57$ (Refs. [64] and [65]).
[b]Experiment: 0.64 (Ref. [68]).

As-Ga and In-Sb at the interface. Overall, there is an expected tendency for the interface bonds to relax toward their natural bond length of bulk lattice. As noted from Table VI, the VBOs for relaxed heterojunctions generally differ from those for the unrelaxed heterojunctions (see Tables III and IV) by a significant amount of ∼0.2–0.8 eV. Importantly, without any interface relaxation, heterojunctions are found to have VBOs that are approximately independent of the interface orientation or interface bond identity, as discussed above. But even with the interface structure relaxed significantly from the clamped structure and, furthermore, relaxed differently for different cation-anion pairs at the interface, it is interesting to find that the VBO is still largely insensitive to the interface orientation and interface bond identity, as shown in Table VI [68].

Because the VBO is directly related to the interface charge distribution through the interface dipole contribution noted in Eq. (1), a successful model for explaining these results must therefore rest with the ability to understand and predict the effect of relaxation on charge distribution. The localness in electron density variation, discovered for all heterojunctions in the present paper, suggests that the electrostatic effect associated with lattice relaxation may itself be largely local. In other words, a semiquantitative theory of how, e.g., the charge density in a "1.5 1.5" cell changes with lattice relaxation should suffice. The variation in the local charge density associated with energy minimization, however, is still nontrivial, as it involves changes in bond lengths and angles. Nevertheless, a reasonable guess of the equilibrium charge distribution for relaxed interfaces may consist of charge densities from distorted quadrants. With this observation, the stage is finally set for the introduction of the NPT, which is a surprise find in the present investigation.

VI. NEUTRAL POLYHEDRA THEORY

To formulate relaxation effects into a more general theory, consider first how the distribution of charge inside a quadrant changes with quadrant dimension. The dependence of the calculated quadrant dipole moment on the ZB lattice parameter for several semiconductors is shown in Fig. 14. Note that unlike in Fig. 11, here (as well as in Figs. 15–17 below), the calculation is for *single* quadrant, not a layer of quadrants. Clearly, the dipole moment of the quadrant gradually decreases with increasing lattice parameter and bond length increase.

To analyze the formation of the total dipole moment in detail, the accumulated dipole, $P(x)$, defined as [56]

$$P(x) = \int_{-\infty}^{x} dx'(x' - x) \iint dydz\rho(x', y, z), \qquad (2)$$

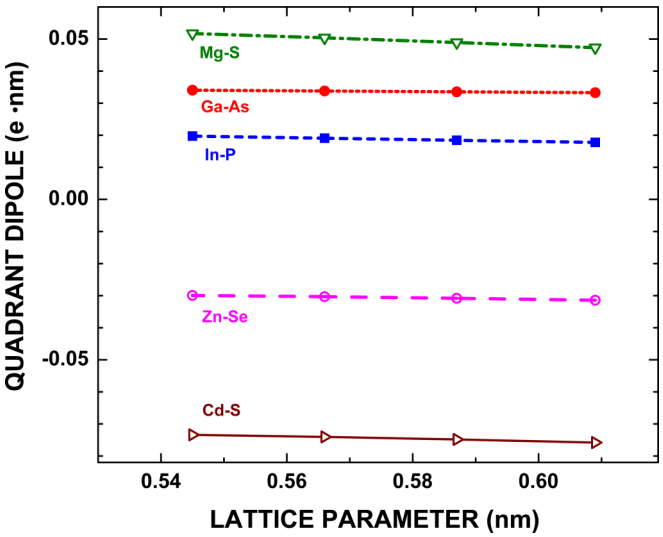

FIG. 14. Dipole moment along the [111] (cation-to-anion) direction of single quadrant of a ZB semiconductor as a function of lattice parameter.

where the integration is over a *single* quadrant, is shown in Fig. 15 along the length of the Mg-S quadrant, calculated for several different lattice parameters. The figure reveals that the decrease in the overall dipole moment with lattice parameter is largely attributable to a decreased (i.e., more negative) dipole moment in the cation half of the quadrant. Recall that, as explained above and shown in Fig. 3(c), each quadrant contains ¼ anion, ¼ cation, and two valence electrons. Because the accumulated dipole reaches its minimum when the accumulated charge, from either side, vanishes, the section of the quadrant in Fig. 15 from Mg to the minimum of the accumulated dipole must contains only 0.5

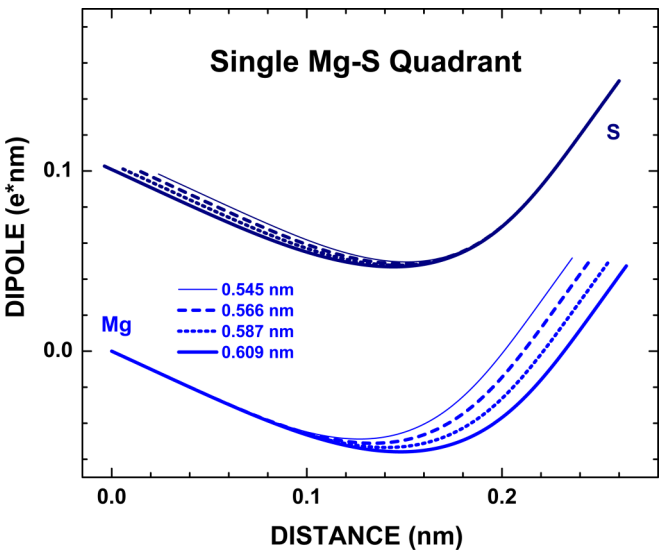

FIG. 15. Accumulated dipole moment [see Eq. (2) of text for definition] of a Mg-S single quadrant, along the length of the quadrant, integrated from the S end (upper) and from the Mg end (lower) of the quadrant, for different lattice parameters. The upper curves have been vertically shifted by 0.15 e nm.

of an electron, while the remaining 1.5 electrons are in the anion half of the quadrant [56]. Analogously, quadrants for III-V semiconductors would have 0.75 and 1.25 electrons, respectively, for cation- and anion-sections (halves) defined in this fashion. Because the charge distribution in the anion half of the quadrant is not significantly affected by a variation in the lattice parameter, or its contribution to the accumulated dipole moment would have changed, one can phenomenologically characterize the energy minimization process as dependent more heavily on charge rearrangement in the cation half of the quadrant. Such a simplified view on the formation of the equilibrium quadrant dipole raises the possibility that the cation side of the quadrant may also end up with a dipole moment that is characteristic only of the cation, upon energy minimization, i.e., when the charge density of quadrant with the optimal (energy minimizing) lattice parameter is used. This possibility turns out to be amazingly real. Accumulated dipole distributions for III-V and II-VI semiconductor quadrants, calculated at their equilibrium lattice parameters, are presented in Fig. 16. They show that the dipole moment for the cation section of the quadrant becomes essentially independent of the anion when the quadrant reaches its equilibrium length. Combined with the earlier observation that the dipole moment for the anion side of the quadrant is approximately independent of the cation, this finding suggests that the dipole moment for a quadrant in its optimum dimension is separable into two parts that each depends only on one element. This key result for comprehensive modeling of VBO at relaxed heterojunctions is demonstrated in Fig. 17, where curves from Fig. 16 are replotted with the minimum of each curve rigidly shifted to the origin. The fact that all dipole curves for a particular element, either cation or anion, end up with approximately the same height indicates the separability of the quadrant dipole moment into two parts.

Figure 17 brings to light an additional crucial point: All dipole curves for an element end roughly at the same location on the length axis, i.e., the length of a cation section in equilibrium is essentially independent of its anion partner, and vice versa! The equilibrium bond length for any of these ZB semiconductors is, therefore, the sum of additive lengths, or radii, of the two elements. Because the minimum in each dipole distribution curve is the neutral point for that quadrant, the individual radius so determined for an element is possibly identifiable with its covalent radius [69,70]. The covalent radii for all elements presently determined from dipole profile are in reasonable agreement with the reported single bond molecular covalent radii [70,71] and the covalent radii for solids [72], as shown in Table VII. This is remarkable given that the covalent radius is arrived at in the present paper on the basis of electrostatic argumentation, which is entirely different from the statistical fitting basis employed in previous studies. The numerical breakdown of the bond length, dipole moment, and potential energy change of a semiconductor quadrant into parts associated with the cation and the anion is given in detail in Table VIII.

With knowledge on the formation of the quadrant dipole from the perspective of energy minimization in hand, we can now consider how BOs are influenced by lattice relaxation. The surprising discovery is that upon energy minimization, the charge density within some neutral region, or neutral

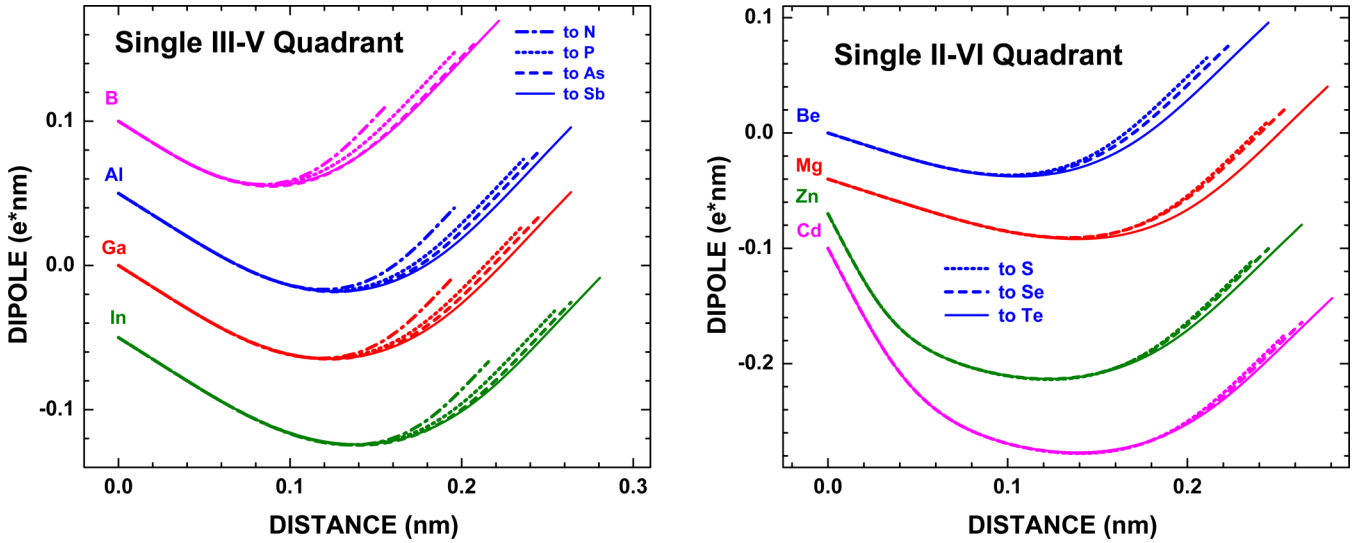

FIG. 16. Dipole moment accumulated from the cation end of selected (a) III-V semiconductors and (b) II-VI semiconductor ZB quadrants, calculated at the equilibrium lattice parameter of each semiconductor. For clarity, curves have been vertically shifted.

polyhedron, up to the covalent radius in bond directions, of each cation or anion appears to converge toward some individually optimized spatial distribution, as reflected by a distinctive dipole moment in the quadrant. This simple outcome in the distribution of charge clearly originates from complex laws of quantum physics that govern the formation of energy-minimized charge density not only in bulk semiconductors but in all electronic systems. It is thus expected that even when bonds are relaxed out of tetrahedral directions, the neutral polyhedra around cations (anions) will still approximately maintain the same spatial distributions, as found to energy minimize the bulk semiconductors. The usual view of the lattice relaxation process is "the approximate restoration of interface bonds to their optimal lengths," which is also a feat that is automatically achieved if the neutral polyhedra around each cation and anion are allowed to approximately reach their respective covalent radii in bond directions. Therefore, a proposal that would simultaneously permit the relaxation of atomic positions toward optimal length for interface bonds and would allow the electrons at a relaxed interface to distribute in a manner that minimizes its energy is to let the charge distribution within the neutral polyhedra around each cation and anion (at the interface) to approximately remain bulklike.

Rooted in the minimization requirement for the interface energy, the above assumption can serve as the underpinning for a simple theory for the formation of BO at both relaxed and unrelaxed heterojunctions. Basically, the charge distribution at any heterojunction can be regarded as being put together with neutral polyhedra, which are volumes around ionic positions that are each electrically neutral. An example of a neutral polyhedron about a cation, obtained by dissecting all four quadrants of this cation at the neutral plane of each quadrant and keeping only the parts belonging to this cation, is shown in Fig. 2(d). The shape of neutral

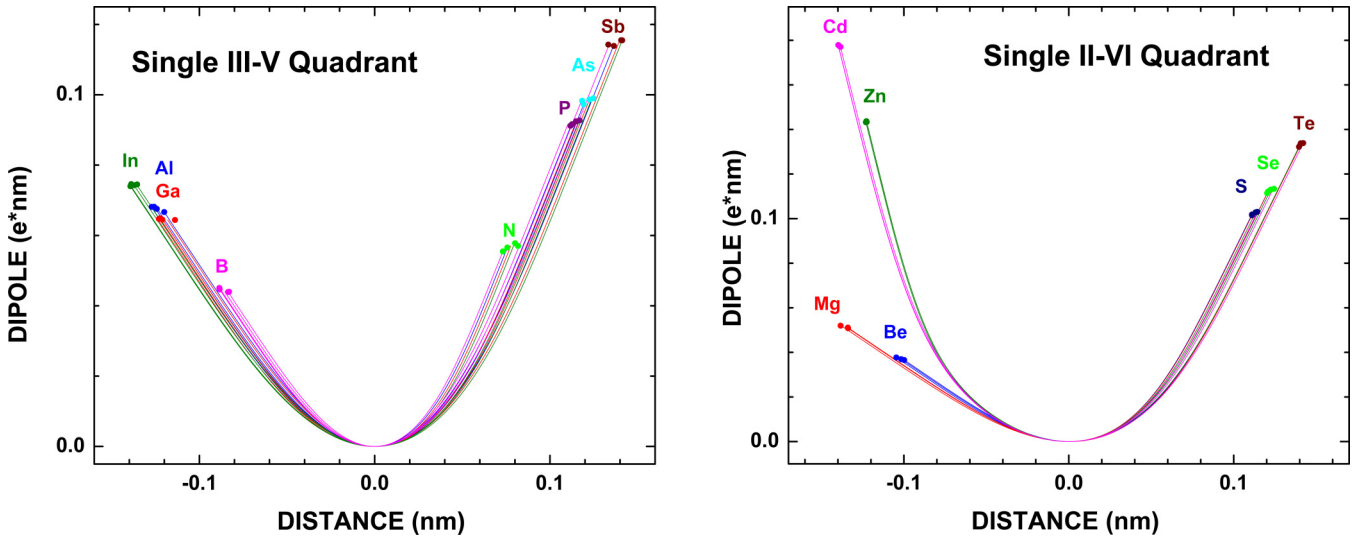

FIG. 17. Accumulated dipole moment curves of the ZB semiconductors from Fig. 16, redisplayed with the neutral point for each quadrant shifted to origin. For clarity, the end points of each curve are marked by dots. (a) III-V semiconductors; (b) II-VI semiconductors.

TABLE VII. The distance from an atom to the neutral point of the quadrant (nm), determined from the present paper. Comparison is made with the covalent radius (C. R., in nm) fitted in single-bond molecules (Ref. [70]) and solids (Ref. [71]), and from analysis of the Cambridge Structural Database (Ref. [69]).

Element	Neutral Length (This Work)	Single-Bond C.R.	Solid C.R.	Cambridge Database C.R.
Al	0.125	0.126	0.129	0.121
Ga	0.122	0.124	0.128	0.122
In	0.138	0.142	0.146	0.142
Be	0.102	0.102	0.106	0.096
Mg	0.135	0.139	0.141	0.141
Zn	0.123	0.118	0.130	0.122
Cd	0.139	0.136	0.148	0.144
Si	0.118	0.116	0.118	0.111
Ge	0.123	0.121	0.123	0.120
P	0.115	0.111	0.108	0.107
As	0.122	0.121	0.117	0.119
Sb	0.140	0.140	0.136	0.139
S	0.113	0.103	0.104	0.105
Se	0.123	0.116	0.115	0.120
Te	0.141	0.136	0.134	0.138

polyhedra created by this method is topologically related to the proximity cell previously proposed as a convenient charge analysis tool [43]. Each neutral polyhedron at the interface has a size and an internal distribution of charge that approximately replicate these characteristics of neutral polyhedra in bulk semiconductors. For bulk semiconductors, each neutral polyhedron has vanishing net charge and net dipole, the latter because of crystal symmetry. While the idea of stacking neutral polyhedra to construct a model for the heterojunction charge density appears to be chemically sound and practically straightforward, the actual execution is made nontrivial by lattice relaxation. With relaxation in atomic positions, the quadrants at the interface are distorted, and the electrostatic effect of quadrants becomes inaccurate. For example, a change in bond angle leads to a difference in the potential drop across a layer of quadrants, even if the charge distribution in each quadrant remains unchanged. Furthermore, the shift in atomic positions usually makes the total volume of the interface region different from the sum of all neutral regions to be stacked at the interface. Some overlaps or gaps between neighboring neutral polyhedra are therefore unavoidable for relaxed interfaces. However, because any neutral region to be stacked at the interface is already spatially extended to the ionic radius of the ion it houses, the distance in bond directions between the cation-anion pair is automatically set at the nominal equilibrium bond length, as stacked. As a result, along bond directions there would be little overlap or gap between neutral polyhedral, and mismatches between geometrical facets of the stacked neutral polyhedra would be mostly in peripheral areas away from the main skeleton of the network of bonds. Charge rearrangement away from the bonds is not expected to have a significant effect on the overall potential drop across the stacked interface. Therefore, no major problems are anticipated with the use of stacked neutral polyhedra even in the presence of lattice relaxation.

The practical determination of the VBO from a model of stacked neutral polyhedra is mathematically trivial, as it involves only analysis of the charge density of bulk semiconductors. The division of a potential drop or VBO into two parts that each depends only on one of the semiconductors requires that each part be electrically neutral. One notes that the density of a bulk semiconductor can be completely constructed from stacking neutral polyhedra of its constituent ions together. The neutrality of all the building blocks used in such a construction guarantees that any such model solid will be overall neutral and will be neutral on of all its surfaces. Furthermore, because of the absence of a dipole moment for neutral polyhedra at either cation or anion site, all model solids constructed from neutral polyhedra have the same average potential energy irrespective of the exposed species, orientation, or presence of steps on any of the surfaces. Model solids constructed from neutral polyhedra offer a convenient method, through NPT, to estimate the BO of ZB heterojunctions. The VBM position for a model solid constructed with neutral polyhedra is obtained by simply shifting the VBM position for the CWS (or AWS) terminated surface, tabulated in Table I, by the potential energy difference across a layer of the anion (or cation) portion of quadrants, tabulated in Table VIII. For example, the VBM for polyhedra-stacked surfaces of AlAs is 9.957 (Table I) – 12.691 (Table VIII) = –2.734 eV. This and the NPT VBM positions for other semiconductors are shown in Table VIII. The difference in the NPT VBM values of two isovalent semiconductors is the VBO corresponding to the charge density of the heterojunction interface, as stitched from densities of neutral polyhedra. These predictions from the NPT for relaxed heterojunctions are compared with the results of first-principles calculations in Table VI, which shows that additional charge rearrangement leads to adjustment in the final VBO of typically less than ∼0.2 eV from that of the as-stitched configuration. Because the NPT VBM is a bulk property of the semiconductor, the predicted VBO from the NPT is independent of the orientation of the heterojunction or the identity of the interface bonds at polar interfaces, which is largely in agreement with results of experiments and *ab initio* calculations. The NPT is similar in spirit to the model solid theory for BO formation [19], previously constructed by

TABLE VIII. Breakdown of bond length, dipole moment, and potential energy properties of a semiconductor quadrant into neutral parts.

Semiconductor	Distance Cation-Neut. (nm)	Distance Anion-Neut. (nm)	Cation-Neut. Potential Energy (eV)	Anion-Neut. Potential Energy (eV)	Cation-Neut. Dipole Moment (e·nm)	Anion-Neut. Dipole Moment (e·nm)	NPT VBM (eV)
BN	0.084	0.073	13.999	17.683	− 0.0439	− 0.0555	− 0.006
BP	0.083	0.113	8.994	18.742	− 0.0440	− 0.0916	− 0.772
BAs	0.089	0.118	8.244	17.975	− 0.0451	− 0.0983	− 0.898
BSb	0.088	0.133	7.117	18.214	− 0.0446	− 0.1143	− 0.747
AlN	0.120	0.076	13.634	11.565	− 0.0667	− 0.0565	− 2.938
AlP	0.124	0.112	9.505	12.827	− 0.0676	− 0.0912	− 2.792
AlAs	0.126	0.119	8.889	12.691	− 0.0681	− 0.0973	− 2.734
AlSb	0.127	0.137	7.676	12.832	− 0.0681	− 0.1139	− 2.489
GaN	0.114	0.082	13.170	11.662	− 0.0644	− 0.0570	− 2.191
GaP	0.121	0.115	9.075	13.006	− 0.0645	− 0.0924	− 2.489
GaAs	0.123	0.123	8.460	12.867	− 0.0649	− 0.0986	− 2.377
GaSb	0.123	0.141	7.289	13.014	− 0.0647	− 0.1155	− 2.321
InN	0.136	0.080	12.552	9.734	− 0.0745	− 0.0578	− 2.589
InP	0.137	0.117	9.006	11.242	− 0.0743	− 0.0927	− 2.805
InAs	0.139	0.125	8.404	5.655	− 0.0746	− 0.0990	− 2.828
InSb	0.139	0.141	7.365	11.493	− 0.0740	− 0.1155	− 2.675
Si	0.118	0.118	11.369	11.369	− 0.0808	− 0.0808	− 1.984
Ge	0.123	0.123	10.779	10.779	− 0.0826	− 0.0826	− 1.734
BeS	0.100	0.111	6.443	17.941	− 0.0366	− 0.1018	− 3.251
BeSe	0.102	0.121	5.844	17.745	− 0.0369	− 0.1122	− 2.976
BeTe	0.105	0.141	4.917	17.397	− 0.0377	− 0.1334	− 2.869
MgS	0.134	0.111	6.666	13.239	− 0.0511	− 0.1015	− 4.437
MgSe	0.134	0.120	6.165	13.512	− 0.0508	− 0.1114	− 4.134
MgTe	0.138	0.140	5.270	13.403	− 0.0520	− 0.1322	− 3.990
ZnS	0.123	0.113	20.219	14.461	− 0.1437	− 0.1028	− 3.688
ZnSe	0.123	0.123	18.696	14.741	− 0.1433	− 0.1130	− 3.373
ZnTe	0.123	0.141	16.137	15.070	− 0.1432	− 0.1338	− 3.172
CdS	0.140	0.114	21.571	12.493	− 0.1779	− 0.1030	− 3.992
CdSe	0.139	0.125	19.999	12.771	− 0.1775	− 0.1133	− 3.772
CdTe	0.138	0.142	17.618	13.322	− 0.1770	− 0.1339	− 3.494

superposition of atomic densities [73]. An important difference is that the NPT actually employs/generates the equilibrium charge density for bulk semiconductors and heterojunctions.

Although the NPT yields reasonable estimates of VBO, the simple picture upon which such a theory is envisioned to work is not fully accurate. In reality, lattice relaxation at the heterojunction interface involves multiple layers of atoms, and the lengths of bonds at the interface do not necessarily attain their bulk bond lengths. These obvious shortcomings notwithstanding, NPT has the conceptual advantage that it is based on an electron density that approximately minimizes the energy of the heterojunction interface with a relaxed structure that is approximately optimized. One improvement of the NPT that may be easily included would address the disparity in charge densities on the surfaces of neutral polyhedra from different semiconductors. Similar in nature to a problem previously treated for alloys [74,75], such an abrupt discrepancy along the length of a bond will smooth out and in the process cause a shift in the over potential difference and VBO. By assuming the charge difference to dissipate over $\sim 1/2$ of the bond length, such corrections are less than $\sim$0.15 eV for the heterojunctions presently studied. As shown in Table VI, the agreement between NPT and supercell VBOs improves with this correction for some of the heterojunctions.

In keeping with the experimental observation of an approximately bulklike dependence in semiconductor heterojunction BO, previously proposed models for the formation of BO have been essentially based on some chosen properties of bulk semiconductors. These properties vary from energy levels (CNL [21,25], orbital energy [23], bond energy [24,26], deep level energy [22,76], etc.) in the bandgap of the bulk semiconductor to the average potential energy of model solids based on atomic densities [18,19], interstitial position [13], bond point-charge [58], and WS cell [20] of the bulk semiconductor. The difference in the reference energies of the two bulk semiconductors then gives the prediction of BO for the heterojunction in these models. Because of the intimate connection between the BO and the interface charge distribution outlined in Eq. (1), the most conservative interpretation of the experimentally observed bulklike behavior of the VBO is that the difference in the average potential energy across a heterojunction is independent of interface specifics. The experimental observation of the transitivity rule for some heterojunctions then suggests the possibility that the change in potential energy across a heterojunction might be attributable to the difference between two reference potential energies, each representing only one semiconductor. Furthermore, the reference potential energy for one bulk

semiconductor would remain the same, irrespective of the semiconductor partner it forms heterojunction with. For such a scenario to work, each of the semiconductor references or surfaces has to be electrically neutral. Model solids previously constructed with atomic densities or CWS density satisfies the neutrality requirement but are either a crude approximation of the equilibrium bulk charge density [19] or work only on unrelaxed heterojunctions with a common anion [20]. The detailed analysis of the present paper suggests an NPT based on an electron density that approximately minimizes the interface energy with relaxed atomic structure. With it, the insensitivity of VBO to interface specifics at relaxed heterojunctions is also naturally explained. The connection discovered between the NPT and the established concept of covalent radius in chemistry corroborates the appropriateness of this natural choice of model solid. It may appear at first that the procedures presently used to construct model solids in the NPT are limited to semiconductors with the ZB structure and to isovalent heterojunctions. However, there are counterindications. Although the idea emerges from analysis of isovalent ZB heterojunctions, the usefulness of a bulk reference based on neutral polyhedra of equilibrium bulk charge density goes beyond these examples and may apply also to ionic (oxide) semiconductors, an issue we hope to investigate further [57].

The discovery of a method to construct semiconductor solids from neutral polyhedra is not an explanation of, but rather a result of, the underlying physics and chemistry responsible for the bulklike behavior of heterojunction BO observed experimentally. The main reason that NPT, or other model solid theories, can provide reasonable estimates of BO values obtained from experiment or from first-principles calculations is the absence of significant charge rearrangement at the actual heterojunction interface from the assumed, stitched bulk charge densities. As shown throughout this paper, the equilibrium electron density at a (neutral) heterojunction is found to be dominated by local atomic arrangement and therefore is essentially replaceable with the equilibrium electronic density of other (e.g., bulk, LEGO) electronic systems containing the same local atomic arrangement. This close relation between the electron density and the local atomic structure is in good agreement with both the concepts and the practical results of DFT and, certainly for the ZB crystals discussed here, also in good agreement with the concept of bond formation in TB theory.

In principle, the formation of BO at a heterojunction interface can be an intractable process as it involves the equilibration of dissimilar charge densities across an interface, along with the relaxation of atomic positions to minimize the energy. In practice, two factors greatly simplify the situation: (a) a strong influence on the electron density by local atomic arrangement, thus minimizing the extent of charge rearrangement; (b) a separability of the electrostatic effects due to cation and anion at the neutral point (covalent radius) in a quadrant, thus accounting largely for the effect of lattice relaxation. The combination of these factors makes the prediction of the BO from an interface charge density a manageable task. This same combination underpins the apparent insensitivity of the VBO to the orientation, atomic structure, etc. of the interface. Therefore, the apparently bulklike behavior of the VBO originates from the nonbulklike process of charge density equilibration that depends sensitively on the interface atomic structure and other specifics of the interface. This energy minimization process follows the same rules that all other solid and molecular systems follow. Therefore, a significant advantage of the present approach is that there is no need to invoke mechanisms that are specific to semiconductor interfaces.

VII. SUMMARY AND CONCLUSIONS

Because of the strict dependence of the BO of a heterojunction on the distribution of charge at its interface, the formation of BO must be governed by the physical law that controls the charge distribution, namely, energy minimization. The most straightforward approach to model the BO along that rigorous line of thought would begin with a modeling of the energy-minimized charge density of heterojunctions. However, without detailed knowledge on the commonalities of equilibrium densities at semiconductor interfaces, such an approach seems intractable and indeed has not been attempted before. On the experimental side, investigations have found a bulklike behavior of heterojunction BOs, as reflected in the insensitivity of BO to interface orientation and atomic arrangement and the occasional observation of the transitivity rule for BOs of different heterojunctions. On the face of it, the insensitivity of BO to interface specifics seems at odds with mechanisms that are sensitive to the interface charge density and thus has instead inspired suggestions and models that some reference point, e.g., CNL, in the band structure of individual bulk semiconductor drives the formation of BO. The CNL concept has been in wide and frequent use despite the lack of explicit connections between CNL and interface energy. Considerations from TB and DFT concepts make it plausible that the regularity in the charge distributions of semiconductors in the ZB structure may be carried over to the charge densities at their heterojunction interfaces.

First-principles methods have been employed here to calculate the electronic structure of lattice-matched, relaxed and unrelaxed supercells, oligo-cells, and bulk semiconductors in the ZB structure. The results show that the direct approach to understand BO formation, that of modeling the equilibrium charge densities of isovalent heterojunctions, is actually manageable once the equilibrium charge densities in various structures are carefully analyzed, compared, and understood. To facilitate analysis of charge density, the semiconductor volume is divided into subvolumes, or quadrants, that are individually neutral, each housing one sp^3 bond. A comparison of quadrants of a specific cation-anion pair taken from different locations of a structure or from different structures shows that the charge distribution inside a quadrant is nearly independent of the chemical identities of its neighbor quadrants. Therefore, charge distributions in all quadrants of the same cation-anion pair are largely interchangeable. This observation suggests that the equilibrium electron density distribution in these ZB materials is predominantly dependent on the immediate, local atomic structure and raises the possibility that the equilibrium charge densities at heterojunction interfaces may be modeled piecemeal with charge distributions found in bulk semiconductors and oligo-cells.

Indeed, attempts to juxtapose electron densities extracted from bulk semiconductors and oligo-cells were found to reproduce the electron density and VBO calculated from first principles very well for all heterojunctions of different varieties presently investigated. Modeling with densities extracted from only bulk semiconductors, e.g., CWS stitching and 1Q stitching, produce reasonable estimates of the heterojunction densities, although mismatches at these stitching boundaries are noticeable, likely as the result of interactions, ignored in such stitching schemes, between neighboring quadrants of different chemical identities. The more significant of the interquadrant interactions can be accounted for in the modeling process by employing oligo-cells, from which equilibrated neighboring quadrants of different chemical identities are extracted together. As expected, the use of LEGOs, e.g., through "1 1", "2 2" stitching, etc., significantly improves the agreement between simulated and calculated densities for various heterojunctions. When interactions between adjacent quadrants, previously referred to as second nearest neighbors, are included, heterojunction charge densities for unrelaxed interfaces are accurately reproduced by LEGO stitching.

For relaxed interfaces, equilibrium charge densities are also very well simulated, with oligo-cells that include only small portions that are unrelaxed. These findings reinforce the ideas that energy minimization governs the distribution of charge and the formation of VBO at heterojunctions and that the charge distribution (in these structures) is dominated by atomic arrangement in its close proximity. The localness in the dependence of the charge density on atomic structure also manifests itself in calculated VBOs that are insensitive to the orientation of the heterojunction or the identity of the interface bonds, in agreement with experiment. Such a behavior in BO has been described as bulklike previously.

A systematic analysis of the charge distribution in bulk semiconductors reveals a remarkable separability of the electrostatic effect of quadrant into two neutral and transferable parts, associated with the cation and the anion of the quadrant. When a semiconductor quadrant is divided by a plane, oriented perpendicular to the axial (cation-to-anion) direction and positioned such that the net quadrant charge on either side of the plane vanishes, the charge distribution on the anion side of the cut quadrant has a net dipole moment that is nearly independent of the identity of the cation in the quadrant, and vice versa. The bulklike behavior is easily accounted for by the separability in quadrant charge distribution, and the latter is another, more extreme, example of the localness, or nearsightedness [67], in the dependence of the equilibrium charge density on atomic structure. The plane that partitions a semiconductor quadrant into two neutral parts happens to be a distance of approximately the anion (cation) covalent radius away from the anion (cation). Use of these planes, in addition to the quadrant boundaries, divides a ZB crystal into neutral polyhedra centered about every anion and cation, with minimum radius corresponding to the covalent radius of the ion, which stack seamlessly into the entire volume and charge distribution of the crystal. An approximate view of the formation of equilibrium density in bulk semiconductors, oligo-cells, and heterojunctions of the ZB structure, in light of the localness of the density-structure dependence, is that the charge distribution inside each of the polyhedra largely depends only on the identity of its center ion. This simplification leads to a NPT, based on the charge distribution that minimizes the interface energy, which allows the VBOs of relaxed and unrelaxed heterojunctions to be well estimated. These results identify the bulklike behavior observed for semiconductor heterojunctions as a result of the very local dependence of the charge density on atomic structure and, more importantly, reaffirm the main message here that the formation of BO is governed by energy minimization.

ACKNOWLEDGMENTS

We thank Dr. Ariel Biller for his kind assistance with the calculations and Prof. D. Vanderbilt for useful suggestions.

[1] A. Franciosi and C. G. Van de Walle, Surf. Sci. Rep. **25**, 1 (1996).
[2] E. T. Yu, J. O. McCaldin, and T. C. McGill, Solid State Phys. **46**, 1 (1992).
[3] V. V. Afanas'ev, H.-Y. Chou, M. Houssa, A. Stesmans, L. Lamagna, A. Lamperti, A. Molle, B. Vincent, and G. Brammertz, Appl. Phys. Lett. **99**, 172101 (2011).
[4] F. Bernardini, M. Peressi, and V. Fiorentini, Phys. Rev. B **62**, R16302 (2000).
[5] N. E. Christensen, Phys. Rev. B **38**, 12687 (1988).
[6] S. Rubini, E. Milocco, L. Sorba, and A. Franciosi, J. Cryst. Growth. **184-185**, 178 (1998).
[7] T. M. Duc, C. Hsu, and J. P. Faurie, Phys. Rev. Lett. **58**, 1127 (1987).
[8] J. R. Waldrop and R. W. Grant, Phys. Rev. Lett. **43**, 1686 (1979).
[9] X. Wang, J. Xiang, W. Wang, J. Zhang, K. Han, H. Yang, X. Ma, C. Zhao, D. Chen, and T. Ye, Appl. Phys. Lett. **102**, 031605 (2013).
[10] S. Balaz, Z. Zeng, and L. J. Brillson, J. Appl. Phys. **114**, 183701 (2013).
[11] E. Pelucchi, S. Rubini, B. Bonanni, A. Franciosi, and M. Peressi, Appl. Phys. Lett. **78**, 1574 (2001).
[12] R. T. Tung, Mater. Sci. Eng. Rep. **35**, 1 (2001).
[13] W. R. Frensley and H. Kroemer, J. Vac. Sci. Technol. **13**, 810 (1976).
[14] W. R. Frensley and H. Kroemer, Phys. Rev. B **16**, 2642 (1977).
[15] W. A. Harrison, J. Vac. Sci. Technol. **14**, 1016 (1977).
[16] W. A. Harrison, Phys. Rev. B **24**, 5835 (1981).
[17] E. A. Kraut, J. Vac. Sci. Technol. B **2**, 486 (1984).
[18] C. G. Van de Walle and R. M. Martin, J. Vac. Sci. Technol. A **4**, 1055 (1986).
[19] C. G. Van de Walle and R. M. Martin, Phys. Rev. B **35**, 8154 (1987).
[20] A. Baldereschi, S. Baroni, and R. Resta, Phys. Rev. Lett. **61**, 734 (1988).
[21] J. Tersoff, Phys. Rev. B **30**, 4874 (1984).
[22] J. M. Langer and H. Heinrich, Phys. Rev. Lett. **55**, 1414 (1985).
[23] W. A. Harrison and J. Tersoff, J. Vac. Sci. Technol. B **4**, 1068 (1986).

[24] I. Lefebvre, M. Lannoo, C. Priester, G. Allan, and C. Delerue, Phys. Rev. B **36**, 1336 (1987).
[25] M. Cardona and N. E. Christensen, Phys. Rev. B **35**, 6182 (1987).
[26] R.-Z. Wang, S.-H. Ke, and M.-C. Huang, J. Phys.: Condens. Matter **4**, 8083 (1992).
[27] A. D. Katnani and G. Margaritondo, J. Appl. Phys. **54**, 2522 (1983).
[28] Y. Hinuma, A. Grüneis, G. Kresse, and F. Oba, Phys. Rev. B **90**, 155405 (2014).
[29] P. Hohenberg and W. Kohn, Phys. Rev. **136**, B864 (1964).
[30] W. A. Harrison, Phys. Rev. B **8**, 4487 (1973).
[31] S. T. Pantelides and W. A. Harrison, Phys. Rev. B **11**, 3006 (1975).
[32] N. J. Shevchik, J. Tejeda, and M. Cardona, Phys. Rev. B **9**, 2627 (1974).
[33] N. Marzari and D. Vanderbilt, Phys. Rev. B **56**, 12847 (1997).
[34] N. Marzari, A. A. Mostofi, J. R. Yates, I. Souza, and D. Vanderbilt, Rev. Mod. Phys. **84**, 1419 (2012).
[35] G. Kresse and J. Hafner, Phys. Rev. B **49**, 14251 (1994).
[36] G. Kresse and J. Furthmuller, Phys. Rev. B **54**, 11169 (1996).
[37] G. Kresse and D. Joubert, Phys. Rev. B **59**, 1758 (1999).
[38] J. P. Perdew, K. Burke, and M. Ernzerhof, Phys. Rev. Lett. **77**, 3865 (1996).
[39] R. S. Mulliken, J. Chem. Phys. **23**, 1833 (1955).
[40] F. L. Hirshfeld, Theor. Chim. Acta **44**, 129 (1977).
[41] R. F. W. Bader, Acc. Chem. Res. **18**, 9 (1985).
[42] A. Savin, R. Nesper, S. Wengert, and T. F. Fassler, Angew. Chem. Int. Ed. Engl. **36**, 1808 (1997).
[43] R. T. Tung, Appl. Phys. Rev. **1**, 011304 (2014).
[44] R. Resta, S. Baroni, and A. Baldereschi, Superlatt. Microstr. **6**, 31 (1989).
[45] J. Batey and S. L. Wright, J. Appl. Phys. **59**, 200 (1986).
[46] J. Menéndez, A. Pinczuk, D. J. Werder, A. C. Gossard, and J. H. English, Phys. Rev. B **33**, 8863 (1986).
[47] W. I. Wang and F. Stern, J. Vac. Sci. Technol. B **3**, 1280 (1985).
[48] S. Nagao, T. Fujimori, H. Gotoh, H. Fukushima, T. Takano, H. Ito, S. Koshihara, and F. Minami, J. Appl. Phys. **81**, 1417 (1997).
[49] J. R. Waldrop, R. W. Grant, S. P. Kowalczyk, and E. A. Kraut, J. Vac. Sci. Technol. A **3**, 835 (1985).
[50] W. R. L. Lambrecht and B. Segall, Phys. Rev. B **41**, 8353 (1990).
[51] G. J. Gualtieri, G. P. Schwartz, R. G. Nuzzo, and W. A. Sunder, Appl. Phys. Lett. **49**, 1037 (1986).
[52] J. Menéndez, A. Pinczuk, D. J. Werder, J. P. Valladares, T. H. Chiu, and W. T. Tsang, Solid State Commun. **61**, 703 (1987).
[53] E. T. Yu, M. C. Phillips, D. H. Chow, D. A. Collins, M. W. Wang, J. O. McCaldin, and T. C. McGill, Phys. Rev. B **46**, 13379 (1992).
[54] M. Peressi, N. Binggeli, and A. Baldereschi, J. Phys. D **31**, 1273 (1998).
[55] R. M. Martin, Phys. Rev. B **9**, 1998 (1974).
[56] A. Natan, L. Kronik, and Y. Shapira, Appl. Surf. Sci. **252**, 7608 (2006).
[57] R. T. Tung and L. Kronik (unpublished).
[58] W. R. Frensley, J. Vac. Sci. Technol. **15**, 1465 (1978).
[59] W. A. Harrison, E. A. Kraut, J. R. Waldrop, and R. W. Grant, Phys. Rev. B **18**, 4402 (1978).
[60] R. G. Dandrea, C. B. Duke, and A. Zunger, J. Vac. Sci. Technol. B **10**, 1744 (1992).
[61] Y. Foulon, C. Priester, G. Allan, J. C. Garcia, and J. P. Landesman, J. Vac. Sci. Technol. B **10**, 1754 (1992).
[62] B. Montanari, M. Peressi, S. Baroni, and E. Molinari, Appl. Phys. Lett. **69**, 3218 (1996).
[63] M. S. Hybertsen, Phys. Rev. Lett. **64**, 555 (1990).
[64] G. J. Gualtieri, G. P. Schwartz, R. G. Nuzzo, R. J. Malik, and J. F. Walker, J. Appl. Phys. **61**, 5337 (1987).
[65] G. A. Sai-Halasz, L. L. Chang, J. M. Welter, C. A. Chang, and L. Esaki, Solid State Commun. **27**, 935 (1978).
[66] R. A. McKee, F. J. Walker, M. B. Nardelli, W. A. Shelton, and G. M. Stocks, Science **300**, 1726 (2003).
[67] W. Kohn, Phys. Rev. Lett. **76**, 3168 (1996).
[68] E. T. Yu, M. C. Phillips, J. O. McCaldin, and T. C. McGill, J. Vac. Sci. Technol. B **9**, 2233 (1991).
[69] F. H. Allen, O. Kennard, D. G. Watson, L. Brammer, A. G. Orpen, and R. Taylor, J. Chem. Soc. Perkin Trans. 2 S1 (1987).
[70] B. Cordero, V. Gómez, A. E. Platero-Prats, M. Revés, J. Echeverría, E. Cremades, F. Barragán, and S. Alvarez, Dalton Trans. 2832 (2008).
[71] P. Pyykkö and M. Atsumi, Chemistry - A European Journal **15**, 186 (2009).
[72] P. Pyykkö, Phys. Rev. B **85**, 024115 (2012).
[73] L. F. Mattheiss, Phys. Rev. **134**, A970 (1964).
[74] A. R. Miedema, P. F. de Chatel, and F. R. de Boer, Physica B & C **100**, 1 (1980).
[75] F. R. de Boer, R. Boom, W. C. M. Mattens, A. R. Miedema, and A. K. Niessen, *Cohesion in Metals: Transition Metal Alloys*, 711 (Amsterdam, North-Holland, 1988).
[76] J. Tersoff and W. A. Harrison, Phys. Rev. Lett. **58**, 2367 (1987).